

Out-of-equilibrium dynamics of repulsive ranked diffusions: The expanding crystalAna Flack,¹ Pierre Le Doussal,² Satya N. Majumdar,¹ and Grégory Schehr³¹*LPTMS, CNRS, Université Paris-Sud, Université Paris-Saclay, 91405 Orsay, France*²*Laboratoire de Physique de l'Ecole Normale Supérieure, CNRS, ENS and PSL Université, Sorbonne Université, and Université Paris Cité, 24 Rue Lhomond, 75005 Paris, France*³*Laboratoire de Physique Théorique et Hautes Energies, CNRS UMR No. 7589, Sorbonne Université, 4 Place Jussieu, 75252 Paris Cedex 05, France*

(Received 6 March 2023; accepted 5 May 2023; published 5 June 2023)

We study the nonequilibrium Langevin dynamics of N particles in one dimension with Coulomb repulsive linear interactions. This is a dynamical version of the so-called jellium model (without confinement) also known as ranked diffusion. Using a mapping to the Lieb-Liniger model of quantum bosons, we obtain an exact formula for the joint distribution of the positions of the N particles at time t , all starting from the origin. A saddle-point analysis shows that the system converges at long time to a linearly expanding crystal. Properly rescaled, this dynamical state resembles the equilibrium crystal in a time-dependent effective quadratic potential. This analogy allows us to study the fluctuations around the perfect crystal, which, to leading order, are Gaussian. There are however deviations from this Gaussian behavior, which embody long-range correlations of purely dynamical origin, characterized by the higher-order cumulants of, e.g., the gaps between the particles, which we calculate exactly. We complement these results using a recent approach by one of us in terms of a noisy Burgers equation. In the large- N limit, the mean density of the gas can be obtained at any time from the solution of a deterministic viscous Burgers equation. This approach provides a quantitative description of the dense regime at shorter times. Our predictions are in good agreement with numerical simulations for finite and large N .

DOI: [10.1103/PhysRevE.107.064105](https://doi.org/10.1103/PhysRevE.107.064105)**I. INTRODUCTION AND MAIN RESULTS**

The Coulomb potential in one dimension is linear in the distance. Particles interacting with this potential have been much studied. Many of these studies address the canonical equilibrium at some temperature T . In the attractive case it is related to the statistical mechanics of the self-gravitating one-dimensional (1D) gas [1–3]. In the repulsive case, in the presence of a background charge or in a finite box, it is called jellium and its fluctuations at equilibrium have been well studied [4–9], with a recent renewed interest, in particular, in edge fluctuations and large deviations [10–14].

In this paper we study the out-of-equilibrium dynamics of this system and demonstrate that it exhibits rather rich and interesting behaviors, as a function of time. In one dimension, the Coulomb force (either attractive or repulsive) acting on each particle is proportional to its rank, i.e., the number of particles in its front minus the number of particles at the back of it. The Langevin dynamics of this system is called ranked diffusion. The diffusion of N particles in one dimension under a drift which depends only on their ranks has been studied in finance [15] and in mathematics [16,17].

Recently, the nonequilibrium dynamics of this model was studied [18] using a mapping to the Lieb-Liniger model, or 1D delta Bose gas. Since the latter is integrable by the Bethe ansatz, in principle it allows one to obtain a formula for nonequilibrium observables in the ranked diffusion model for any N . In practice, however, this approach is analytically complicated and not all initial conditions can be easily treated. Hence this program has yet to be fully completed.

Furthermore, the exact solution does not allow one to add an external potential, since it breaks integrability. Another more versatile approach was thus also studied in [18], which exploits a connection to the noisy Burgers equation. This method is most efficient to study the large- N limit, where the effect of the noise term is reduced.

In this paper we focus on the repulsive gas and show that many exact results on its dynamics can be derived using the two aforementioned complementary approaches. We study a gas of N particles on the line, in the absence of an external potential, performing thermal diffusion at temperature T , and mutually interacting via the linear Coulomb potential of strength $c > 0$ [see the definition of the model in (4)]. In addition to diffusion, each particle thus experiences a drift proportional to its rank, typically of $O(cN)$ for large N . There is no additional hard-core interaction and therefore the particles are free to cross each other. We focus on the case where all the particles start at $t = 0$ from the origin at $x = 0$. Several realizations of this dynamics are shown in Fig. 1 for $N = 500$, where one can see that there are several interesting regimes as a function of time. Since the gas is expanding from a point source, it is dense at short times and particles experience many mutual crossings [see Fig. 1(a)]. At long time, the gas is diluted and the particles are far from each other, but, as we will show, they nevertheless form a well-ordered expanding crystal due to the long-range nature of the interaction [see Fig. 1(c)]. In fact, we find that when N is large one can distinguish *three* different regimes [see Figs. 1(a)–1(c)]. Indeed, there are two characteristic length scales associated with the diffusion and the drift, respectively,

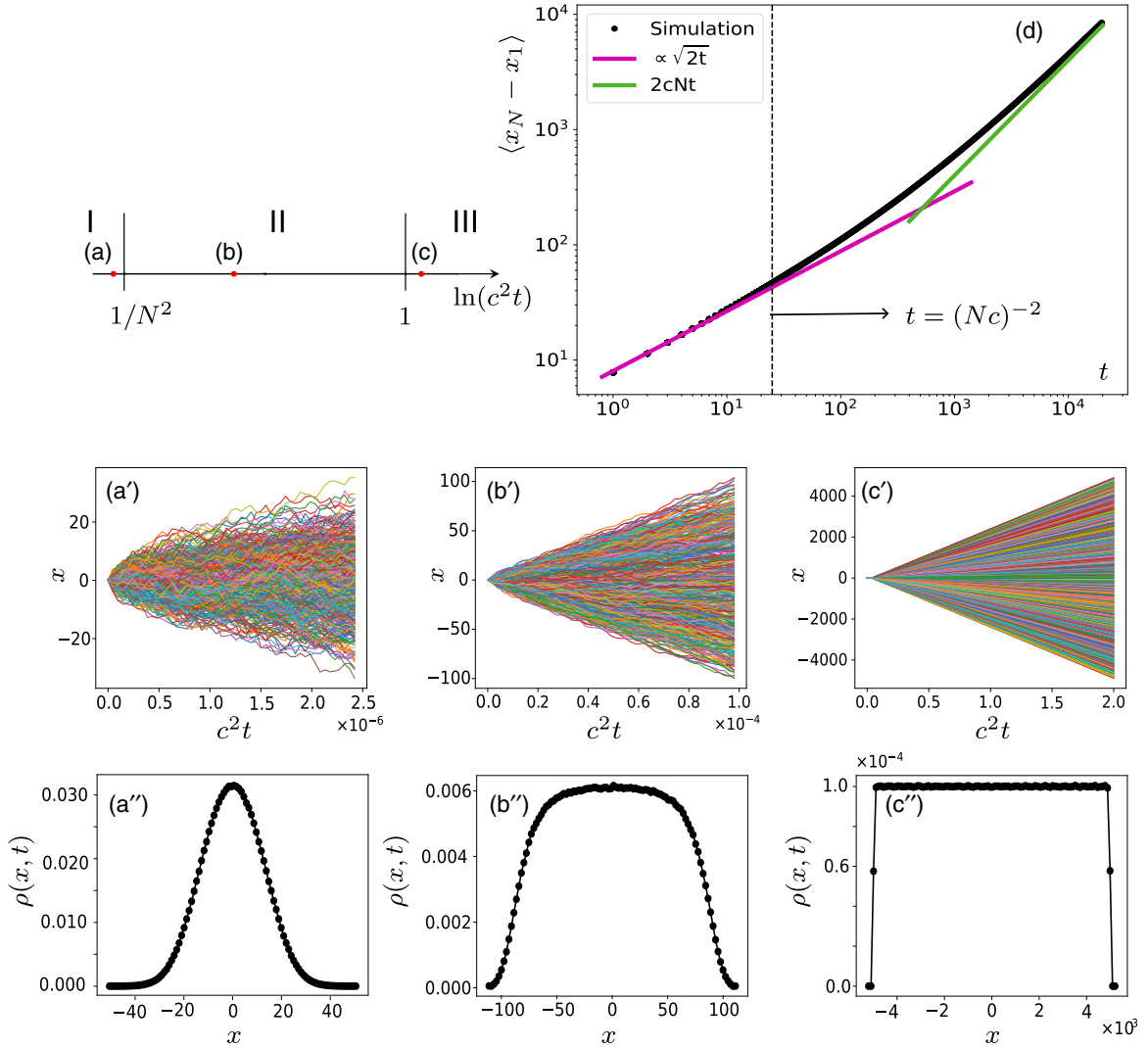


FIG. 1. (a)–(c) Summary of the values of the dimensionless final time c^2t used in (a')–(c') and (a'')–(c''). (d) Size of the gas as a function of time (in ln–ln scale), which shows a crossover between regimes I and II and time $t_1^* = T/(Nc)^2$, which is indicated by a vertical dashed line. Symbols are the results of numerical simulations. The pink solid line at short time represents the prediction in regime I, $\ell_T = \sqrt{2Tt}$ (here $T = 1$), and the green one at longer time corresponds to the prediction in regime II, $\ell = 2Nct$ [see Eq. (1)]. (a')–(c') Examples of trajectories $x_i(t)$ vs t of $N = 500$ particles evolving via the Langevin equation (4). One can identify three different regimes determined by the value of the dimensionless time c^2t . (a'')–(c'') Corresponding densities of particles $\rho(x, t_f)$ at the final time $t = t_f$ for each of (a)–(c). They are obtained by averaging over 10^4 realizations of the noise and using 100 bins to construct the histograms. Here, for convenience, we chose $t_f = 50$ and varied c . These three values fall in each of the three regimes I–III discussed in the text.

namely,

$$\ell_T \sim \sqrt{2Tt}, \quad \ell \sim 2cNt. \quad (1)$$

The first length ℓ_T is the typical thermal diffusion length of independent particles. Since the rightmost (leftmost) particle experiences a drift of approximately cN ($-cN$) the second length ℓ is the total size of the gas at long time. Comparing the two length scales, we see that there is a characteristic timescale

$$t_1^* \sim \frac{1}{N^2} \frac{T}{c^2} \quad (2)$$

such that for $t < t_1^*$ the diffusion dominates over the drift. In that regime, which we call regime I, the particles are

almost independent and the gas is very dense [see Fig. 1(a)]. For time $t > t_1^*$ the drift, i.e., the interaction, dominates over the diffusion. This is regime II, where the gas evolves from being dense to being dilute. The crossover from regime I to regime II in the behavior of the size of the gas (i.e., distance between the rightmost and leftmost particles) is shown in Fig. 1(d). As we will show, in regime II, as time increases, the density converges to a square shape, being uniform over $[-\ell/2, \ell/2]$, with a boundary layer at the two edges of size $\ell_T \sim \sqrt{2Tt} \ll \ell$. In this regime II, however, the particles still experience many crossings [see Fig. 1(b)] and the size of the boundary layer is still much larger than the interparticle distance $a = \ell/N = 2ct$. As time further increases the density becomes so low that the particles cross each other only

rarely. This happens when $a \sim \ell_T$, which defines the second timescale

$$t_2^* \sim \frac{T}{c^2}. \quad (3)$$

Beyond this timescale, for $t \gg t_2^*$, one has $\ell_T \ll a = 2ct$, and the particles are well separated and do not cross anymore; this is regime III (dilute regime). These three regimes, together with the formation of a square density, can be clearly seen in Fig. 1. Note that if the initial condition has instead a finite extension ℓ_0 , there exists another timescale $t_0^* \sim \ell_0/cN$ at which most features of the initial density are erased and the plateau forms. Here we mainly focus on the case $\ell_0 = 0$, so this timescale is absent. Note that for finite N these timescales are all identical and there is only a short-time regime $c^2t/T \ll 1$ and a long-time regime $c^2t/T \gg 1$.

These three regimes exhibit quite different density and particle correlation properties. To obtain a quantitative description of the system, we first derive in Sec. II, using the Bethe ansatz, an integral formula for the joint probability distribution function (PDF) of the positions of the particles, all starting from the origin, given in Eq. (12), which is exact for any N and t . By analyzing this formula via a saddle-point method, we obtain in Sec. III the asymptotic form of the joint PDF at long time [see Eq. (25)]. It is *a priori* valid for any fixed N and for $c^2t/T \gg 1$. At large N it thus describes regime III (the dilute regime). From that formula we find that in that regime the system is a well-ordered expanding crystal, with most probable particle positions $x_j = c(N + 1 - 2j)t$. To compute the fluctuations of the particle positions in this crystal, we proceed in two stages. We first approximate the formula (25) for the joint PDF by neglecting the rational prefactor, in which case it becomes formally identical to the equilibrium distribution given in Eq. (32) of the 1D jellium model [defined in (28)]. Although this analogy holds for any N , it is especially useful for large N , where many results are known for the jellium model [10,11]. We find that, within that approximation, regime III corresponds to the jellium model with a dimensionless interaction strength $\alpha \gg 1$. It correctly predicts the leading order of the fluctuations of the particle positions around their ordered positions, which in this regime are small and independent Gaussian random variables. The amplitude of these fluctuations is of the order of the diffusion length $\ell_T \sim \sqrt{2Tt}$. Next we treat more accurately the asymptotic joint PDF in Eq. (25) and show that there are nontrivial additional position fluctuations, which are of $O(T/c)$. We characterize them completely by computing analytically all the joint cumulants of the particle positions, given in Eq. (68). These formulas show that there are nontrivial correlations of purely dynamical origin, which persist for $c^2t/T \gg 1$ and go beyond the analogy with the equilibrium jellium model. It is yet unclear how to extend these results to the case $c^2t/T = O(1)$ and in particular to the more correlated regime II, i.e., for $c^2t/T \ll 1$, where the particle crossings cannot be ignored. We expect that some of these effects will be captured by the analogy with the jellium model at finite interaction strength α , but that additional dynamical correlations will also exist. Note that we also treat exactly the case $N = 2$, which is quite instructive, in particular, in analyzing systematically the role

of the initial condition (which we were not able to do for general N).

Next, in Sec. IV, we recall the hydrodynamic approach of [18] using the Burgers equation, which gives a prediction for the time-dependent density at large N for arbitrary time. It thus allows us to derive an analytical formula for the time evolution of the average particle density within the crossover between regimes I and II, when the gas is still sufficiently dense. For that study it is convenient to scale $c = \gamma/N$ with $\gamma = O(1)$, in which case the timescale $t_1 = O(1)$. Finally, we perform numerical simulations and compare the results with the predictions of both methods (the Bethe ansatz and the hydrodynamic approach). We confirm the Gaussian character of the fluctuations in regime III and we test the accuracy of the predictions for the density using the deterministic Burgers equation.

Finally, in Appendix A we study in detail the case $N = 2$. In Appendix B we study the corrections to the cumulants of the particle positions, which are exponentially small at long time. In Appendix C we derive the form of the boundary layer for the Burgers equation.

II. MODEL AND MAIN FORMULA

In this paper we consider N particles on the real line at positions $x_i(t)$, $i = 1, \dots, N$, evolving according to the Langevin equation

$$\begin{aligned} \frac{dx_i}{dt} &= -\partial_{x_i} W(\vec{x}) + \sqrt{2T} \xi_i(t) \\ &= -c \sum_{j=1}^N \text{sgn}(x_j - x_i) + \sqrt{2T} \xi_i(t), \end{aligned} \quad (4)$$

where $\xi_i(t)$ are N unit independent white noises with zero mean $\langle \xi_i(t) \rangle = 0$ and delta correlator $\langle \xi_i(t) \xi_j(t') \rangle = \delta_{i,j} \delta(t - t')$. Here T is the temperature and by convention $\text{sgn}(0) = 0$. The particles interact via the linear pairwise potential energy $W(\vec{x}) = -c \sum_{i < j} |x_i - x_j|$, where we define $\vec{x} = \{x_i(t)\}_{i=1, \dots, N}$. The particles may cross (and they will) and if we denote by $x_{(i)}(t)$ the ordered sequence of their positions at time t in increasing order, then the ordered particle $x_{(i)}$ experiences a drift

$$\delta_i = -c \sum_{j=1}^N \text{sgn}(x_{(j)} - x_{(i)}) = -c(N + 1 - 2i), \quad (5)$$

which depends on the label or rank i of the particle, this is just proportional to the number of particles in front minus the number of particles at the back of the i th particle. For $c > 0$ the interaction is thus repulsive, the case considered here.

Next we introduce the PDF $P(\vec{x}, t)$ of a given configuration \vec{x} of the particles. It satisfies the Fokker-Planck equation

$$\partial_t P = -\mathcal{H}_{\text{FP}} P = \sum_i \left(T \partial_{x_i}^2 - c \partial_{x_i} \sum_j \text{sgn}(x_i - x_j) \right) P. \quad (6)$$

For $c < 0$ this equation formally admits a zero-current stationary solution

$$P_0(\vec{x}) = \frac{1}{Z_N} \Psi_0(\vec{x})^2, \quad (7)$$

$$\Psi_0(\vec{x}) := e^{-(1/2T)W(\vec{x})} = \exp\left(\frac{c}{4T} \sum_{i,j=1}^N |x_i - x_j|\right),$$

where Z_N is a normalization constant. For $c > 0$ this solution is however not normalizable and is not the stationary state. Indeed, in the absence of an external potential the gas expands linearly with time [18], an expansion that we will study here in more detail.

It is useful to note at this stage that the two parameters of the model, T and c , can be absorbed in a change of units. More precisely, T/c is a length scale and T/c^2 is a timescale. In terms of these scales one can always write

$$P(\vec{x}, t) = \left(\frac{c}{T}\right)^N \tilde{P}\left(\frac{c\vec{x}}{T}, \frac{c^2 t}{T}\right), \quad (8)$$

where $\tilde{P}(\vec{x}, t)$ is the PDF for the model with $c = T = 1$. We have seen in the Introduction that at large N there are several distinct timescales. These can be explored conveniently by scaling c in various ways with N . Hence we will not fix the parameter c . However, for the calculations in the remainder of this section, as well as in Sec. III, we will set $T = 1$. Since c and T can be absorbed in the units, there is no intrinsic dimensionless parameter in the model, besides N and some parameter characterizing the initial condition, such as $c\ell_0/T$, if ℓ_0 is the initial interparticle distance (below we focus on $\ell_0 = 0$). Hence all the regimes can be obtained by looking at the particular scale of interest.

Let us consider now the δ initial condition where all particles are at the same position $\vec{x}(0) = \vec{0}$ in space at time $t = 0$,

$$P(\vec{x}, t = 0) = \prod_i \delta(x_i). \quad (9)$$

Hence $P(\vec{x}, t)$ is the Green's function of the Fokker-Planck operator \mathcal{H}_{FP} , i.e., $P(\vec{x}, t) = G_{\text{FP}}(\vec{x}, \vec{0}, t)$, where $G_{\text{FP}}(\vec{x}, \vec{y}, t) = \langle \vec{x} | e^{-t\mathcal{H}_{\text{FP}}} | \vec{y} \rangle$. It is easy to check that

$$G_{\text{FP}}(\vec{x}, \vec{y}, t) = \frac{\Psi_0(\vec{x})}{\Psi_0(\vec{y})} G_s(\vec{x}, \vec{y}, t) e^{E_0 t}, \quad (10)$$

with $E_0 = -\frac{c^2}{12}(N^3 - N)$, where $G_s(\vec{x}, \vec{y}, t)$ is the Green's function of the Schrödinger Hamiltonian \mathcal{H}_s , i.e., the solution for $t > 0$ of $\partial_t G_s = -\mathcal{H}_s G_s$ with initial condition $G_s(\vec{x}, \vec{y}, t = 0) = \prod_i \delta(x_i)$. Here \mathcal{H}_s is the Lieb-Liniger Hamiltonian [19]

$$\mathcal{H}_s = -\sum_i \partial_{x_i}^2 + 2c \sum_{1 \leq i < j \leq N} \delta(x_i - x_j), \quad (11)$$

which describes quantum particles with delta repulsive interactions. Note that the initial condition (9) is symmetric in the exchange of particles. In this symmetric sector the model (11) is also called the δ Bose gas, which is integrable by the Bethe ansatz [19,20]. The quantity E_0 is the ground-state energy of the model. The relation (10) can be checked by applying \mathcal{H}_{FP} on each side.

For the δ initial condition the Schrödinger problem can be solved and there exists a multiple integral formula for $G_s(\vec{x}, \vec{0}, t)$ valid for all times. From Proposition 6.2.3 [Eq. (6.6)] in [21] (for earlier works see [20,22]) and using (10), we obtain for $c > 0$, for any N and $t > 0$ and for the sector $x_1 \leq x_2 \leq \dots \leq x_N$,

$$P(\vec{x}, t) = G_{\text{FP}}(\vec{x}, \vec{y} = \vec{0}, t) = \exp\left(\frac{c}{4} \sum_{i,j=1}^N |x_i - x_j| e^{E_0 t}\right) \int_{\mathbb{R}} \frac{dk_1}{2\pi} \dots \times \int_{\mathbb{R}} \frac{dk_N}{2\pi} \prod_{1 \leq a < b \leq N} \frac{ik_a - ik_b}{ik_a - ik_b + c} \times \exp\left(-t \sum_{j=1}^N k_j^2 + i \sum_{j=1}^N x_j k_j\right), \quad (12)$$

where the variables k_i are integrated over the real axis and E_0 is given in Eq. (10). Being a fully symmetric function of its arguments, $P(\vec{x}, t)$ is obtained in the other sectors by symmetry. Note that, by construction, $P(\vec{x}, t)$ in Eq. (12) is normalized to unity on \mathbb{R}^N for all time $t \geq 0$, although this property is not so obvious to check from (12). This explicit expression in Eq. (12) is our main formula, which we analyze in the following sections.

III. TIME EVOLUTION OF $P(\vec{x}, t)$

In this section we analyze the time evolution of $P(\vec{x}, t)$. In Sec. III A we verify the validity of the formula (12) for $N = 2$ by finding directly the exact solution of the Fokker-Planck equation (6). The case $N = 2$ being already very instructive, we study in detail its long-time asymptotics. In Sec. III B we perform a saddle-point analysis of the formula in (12) for large t , for any fixed N . In Sec. III C we make an analogy between this expanding Coulomb gas at large t and the static properties of a one-dimensional one-component plasma in a harmonic potential. Finally, in Sec. III D we obtain the higher cumulants of the position fluctuations from a more precise analysis of the long-time limit.

A. Two particles $N = 2$

Let us start with two particles, i.e., $N = 2$. Introducing the center-of-mass coordinate $x(t) = \frac{1}{2}[x_1(t) + x_2(t)]$ and the relative coordinate $y(t) = x_2(t) - x_1(t)$, the Fokker-Planck equation (6) is easily solved directly by a Laplace transform. Denoting by $P(y, t)$ the PDF of $y(t)$ (with a slight abuse of notation), we find (see details in Appendix A)

$$\tilde{P}(y, s) = \int_0^{+\infty} dt e^{-st} P(y, t) = \frac{e^{(c/2)|y|}}{2(c + \sqrt{c^2 + 2s})} e^{-\sqrt{c^2 + 2s}|y|/2}, \quad (13)$$

which upon Laplace inversion gives

$$P(y, t) = \frac{e^{-(|y|-2ct)^2/8t}}{2\sqrt{2\pi}\sqrt{t}} - \frac{1}{4} c e^{c|y|} \operatorname{erfc}\left(\frac{2ct + |y|}{2\sqrt{2}\sqrt{t}}\right), \quad (14)$$

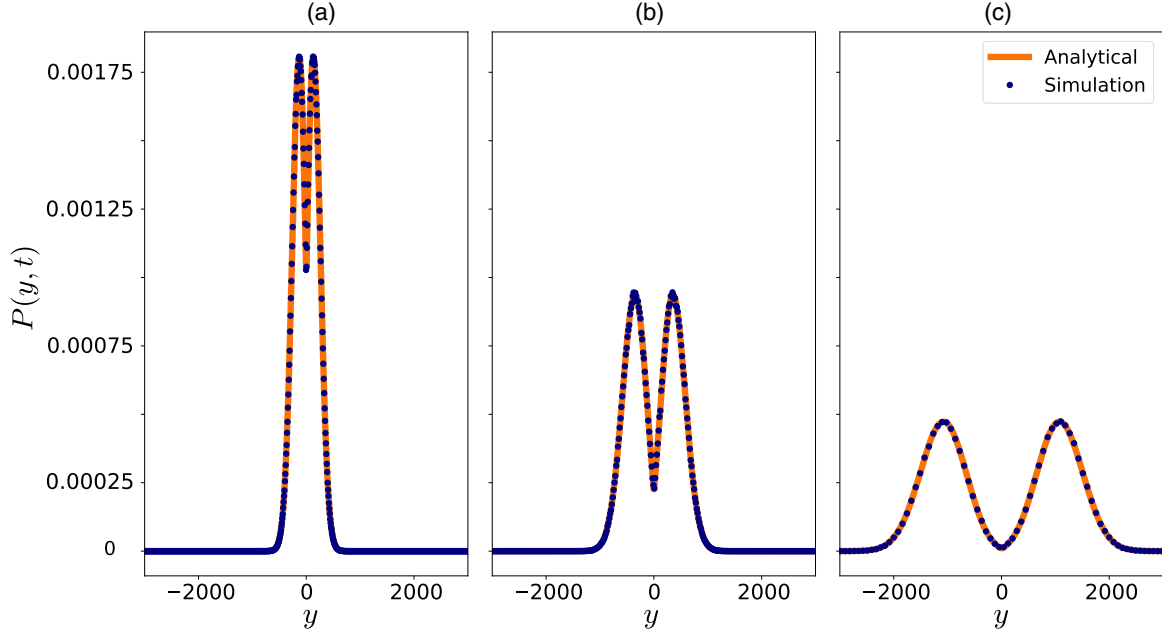


FIG. 2. Probability distribution $P(y, t)$ of the relative coordinate $y(t) = x_2(t) - x_1(t)$ for two particles for different times (a) $t = 5000$, (b) $t = 15000$, and (c) $t = 50000$. The blue dots are obtained by the simulation with $c = 0.01$, $T = 1$, and averaging over 10^6 realizations. The orange solid lines represent the analytical expression for the distribution derived in Eq. (14). One can see that the distribution becomes bimodal at long time.

which is normalized to unity, i.e., $\int_{-\infty}^{+\infty} dy P(y, t) = 1$, and satisfies the initial condition $P(y, 0) = \delta(y)$. Here $\text{erfc}(z) = 2/\sqrt{\pi} \int_z^{\infty} e^{-u^2} du$. We now want to check that the general formula in Eq. (12) for the joint distribution of N particles also leads to the result in Eq. (14) for $N = 2$. Indeed, in Appendix A we show this explicitly. The time evolution of $P(y, t)$ from (14) is plotted in Fig. 2.

At long time it becomes a bimodal distribution centered around $y \simeq \pm 2ct$. For fixed $y = O(1)$ one finds, as $t \rightarrow \infty$,

$$P(y, t) \simeq \frac{(c|y| + 2)e^{-(|y|-2ct)^2/8t}}{4\sqrt{2\pi}c^2t^{3/2}} \simeq \frac{(c|y| + 2)e^{|y|/2}}{4\sqrt{2\pi}c^2t^{3/2}} e^{-c^2t/2}, \quad (15)$$

where in the last equation we used that $|y| = O(1)$. On the other hand, if one scales $y = zt$ with fixed $z = O(1)$ one finds

$$P(y, t) \simeq \frac{|z|e^{-t(|z|-2c)^2/8}}{2\sqrt{2\pi t}(|z| + 2c)}. \quad (16)$$

On these scales it thus converges, as $t \rightarrow \infty$, to a pair of δ functions at $z = \pm 2$, each of weight $\frac{1}{2}$. For t large but finite one can check that the total probability weight in the asymptotic form (16) is slightly less than unity, but converges to unity as $t \rightarrow +\infty$. Note that although the exponential factor is the same in (15) and in (16), the prefactors in each formula are distinct: Only the large $|y| = O(1)$ limit of (15) matches the small $|z| = O(1)$ limit of (16).

One can also calculate the cumulants of the random variable $|y| - 2ct$. While more detailed expressions are given in Appendix A 3, here we simply indicate their leading behaviors

at long time. We obtain

$$\langle |y| \rangle - 2ct \simeq \frac{1}{c} + O(t^{-3/2}e^{-c^2t/2}), \quad (17)$$

$$\langle (|y| - 2ct)^2 \rangle_c \simeq 4t - \frac{3}{c^2} + O(t^{-1/2}e^{-c^2t/2}), \quad (18)$$

$$\langle (|y| - 2ct)^3 \rangle_c \simeq \frac{14}{c^3} + O(t^{1/2}e^{-c^2t/2}), \quad (19)$$

$$\langle (|y| - 2ct)^4 \rangle_c \simeq -\frac{90}{c^4} + O(t^{3/2}e^{-c^2t/2}), \quad (20)$$

where $\langle \dots \rangle_c$, with a subscript c , denotes cumulants (not to be confused with the interaction parameter c). Interestingly, while the variance of $|y|$ grows linearly with t for large t , the higher cumulants converge to a constant. The leading fluctuations are thus Gaussian and diffusive $O(\sqrt{t})$, but there are some additional $O(1)$ non-Gaussian fluctuations, as encoded in the higher-order cumulants. As we will see below, these features will extend to any N ; hence $N = 2$ is a useful testing ground for general N . One can check (e.g., numerically) that the leading orders [i.e., up to $O(1)$] of the cumulants (17)–(20) are reproduced if one uses the asymptotic form (16), which thus captures the $O(1)$ non-Gaussian fluctuations at long time. In addition, in Sec. III D we obtain an *exact formula* for the $O(1)$ leading orders of all the cumulants at long time, i.e., for any N (hence including $N = 2$), based on a saddle-point method. To obtain them we show that for $c^2t \gg 1$ one can restrict the study to an ordered sector $x_1 < \dots < x_N$ and neglect the events when particles cross. These events are only responsible for the exponential corrections to the cumulants [e.g., $e^{-c^2t/2}$ for $N = 2$ in (17)–(20)]. Finally, we have checked the predictions of (17)–(20) by a numerical solution of the Langevin equation; the results are presented in Fig. 3.

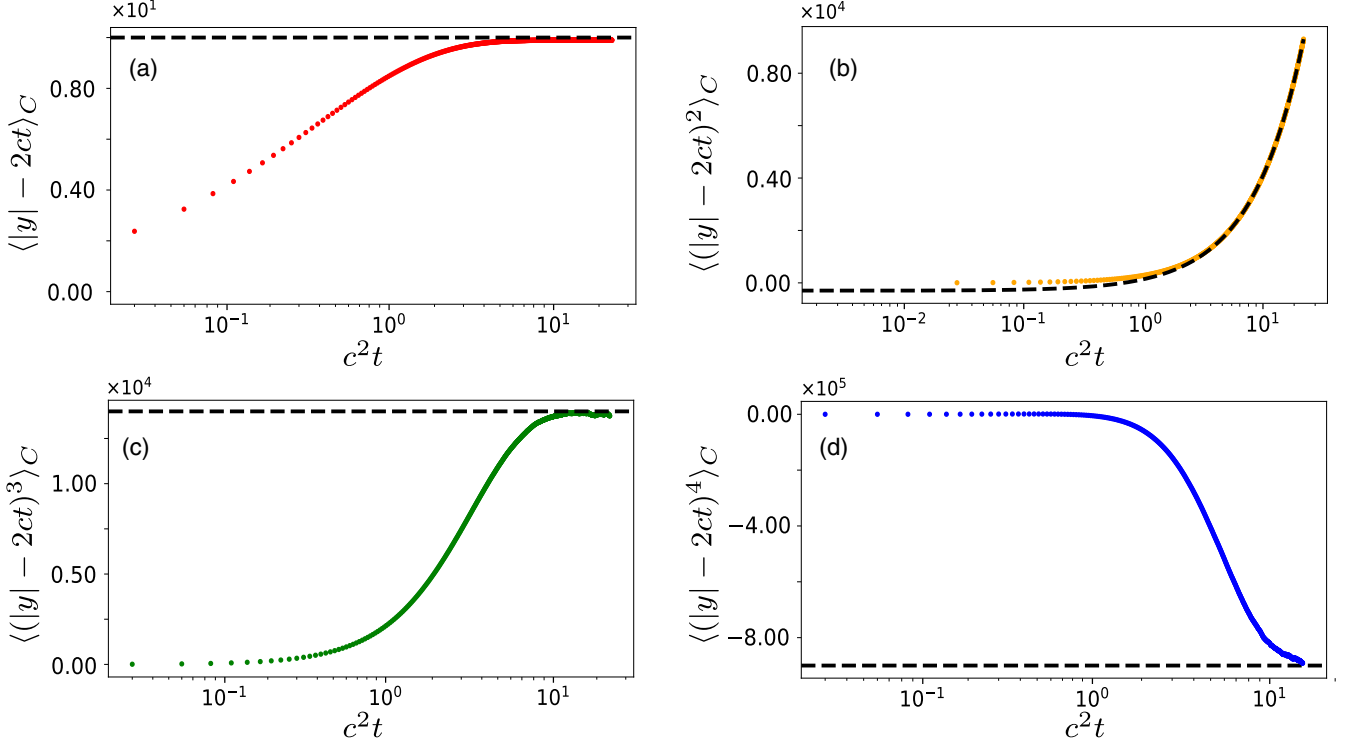


FIG. 3. Plot of first four cumulants $\langle (|y| - 2ct)^k \rangle_C$, with (a) $k = 1$, (b) $k = 2$, (c) $k = 3$, and (d) $k = 4$, as a function of dimensionless time $c^2 t$ (in the scale of the natural logarithm) from the numerical solution of the Langevin equation, compared to the analytical prediction at long time from Eqs. (17)–(20) (black dashed line). We chose $c = 0.1$ and averaged over 2×10^8 realizations of the noise.

B. Saddle-point analysis at late times t for fixed N

Let us now consider the general case of N particles. We start from the general formula (12) for the joint PDF restricted to the sector $x_1 \leq x_2 \leq \dots \leq x_N$. Let us define the rescaled variables $x_j = z_j t$. In terms of these variables the joint PDF $P(\vec{x}, t)$ reads, using E_0 from Eq. (10) and with $z_1 \leq z_2 \leq \dots \leq z_N$,

$$P(\vec{x}, t) = \int_{\mathbb{R}} \frac{dk_1}{2\pi} \dots \int_{\mathbb{R}} \frac{dk_N}{2\pi} \exp \left[t \left(\frac{c}{4} \sum_{i,j=1}^N |z_i - z_j| - \sum_{j=1}^N k_j^2 + i \sum_{j=1}^N z_j k_j - \frac{c^2}{12} N(N^2 - 1) \right) \right] \prod_{1 \leq a < b \leq N} \frac{ik_a - ik_b}{ik_a - ik_b + c}. \quad (21)$$

Let us consider now the regime of long time, $t \rightarrow +\infty$ with fixed N and with $z_j = O(1)$, i.e., $x_j = O(t)$. For long t , the expression multiplying t in the exponent of the integrand in Eq. (21) gets minimized at the saddle point with the values

$$k_j^* = \frac{iz_j}{2}, \quad (22)$$

which are on the imaginary k axis. Note that the original integrals in (21) are on the real k axis. Hence we need to deform the contour in the complex k plane so that it passes through the saddle point and picks up the leading contribution for long t . This can be done without crossing the poles in the prefactor in (21), by deforming the contours for each k_j successively maintaining the condition $\text{Im } k_N > \dots > \text{Im } k_1$. This gives

$$P(\vec{x}, t) \simeq \frac{1}{(4\pi t)^{N/2}} \exp \left(\frac{tc}{4} \sum_{i,j=1}^N |z_i - z_j| - t \sum_j \frac{z_j^2}{4} e^{-(c^2/12)N(N^2-1)t} \right) \prod_{1 \leq a < b \leq N} \frac{z_b - z_a}{z_b - z_a + 2c}. \quad (23)$$

Note that since $z_b > z_a$ for $b > a$ there are no poles in the double product. For $N = 2$ one can check that one recovers the expression in (16), which is a bimodal distribution at long time. As was discussed there, it is valid for $c^2 t \gg 1$, and so is (23) for any finite N .

One can rewrite this formula to make more explicit the most probable position of each particle. Using the equality, for $z_1 \leq z_2 \leq \dots \leq z_N$,

$$\frac{c}{4} \sum_{i,j=1}^N |z_i - z_j| = -\frac{c}{2} \sum_{j=1}^N (N+1-2j)z_j \quad (24)$$

and completing the square, one finds

$$P(\vec{x}, t) \simeq \frac{1}{(4\pi t)^{N/2}} \exp\left(-\frac{t}{4} \sum_{j=1}^N [z_j - c(2j - N - 1)]^2\right) \prod_{1 \leq a < b \leq N} \frac{z_b - z_a}{z_b - z_a + 2c} \quad \text{for } z_1 \leq z_2 \leq \dots \leq z_N. \quad (25)$$

The most probable values for the rescaled positions at long time are thus

$$\frac{x_j}{t} = z_j = c(2j - N - 1). \quad (26)$$

These positions form a perfect crystal with uniform spacing $2c$ which extends from $z_1 = -c(N - 1)$ to $z_N = c(N - 1)$. One can check that for $t \rightarrow +\infty$ the normalization of the formula (25) inside the ordered sector is $1/N!$, as expected. Indeed, in that limit (i) the fluctuations of the z_j 's around the most probable values are vanishing as $1/\sqrt{t}$ and (ii) in the prefactor one can simply replace the z_a by their most probable values $z_a = c(2j - N - 1)$ and one finds that the double product over a and b in (25) simply equals $1/N!$.

We will now, and in the following sections, investigate the deviations around the perfect crystal. Let us define them as

$$\delta x_j = x_j - ct(2j - N - 1). \quad (27)$$

The quadratic form in the exponential in (25) can be rewritten simply as $-\sum_j \frac{\delta x_j^2}{4t}$. This would suggest that the fluctuations of the δx_j 's are independent and Gaussian for each particle with a width given by the diffusion length $\ell_T = \sqrt{2t}$, independently of N . This is *not the case*, however, for the two following reasons: (i) There is an ordering condition between the particles and (ii) there is the double product prefactor in (25).

Nevertheless, it is true that if one scales $\delta x_j = \sqrt{2t} \delta \tilde{x}_j$ with $\delta \tilde{x}_j = O(1)$ the joint PDF of the $\delta \tilde{x}_j$'s converges, as $c^2 t \rightarrow +\infty$, to a product of independent standard Gaussian variables. Indeed, with that scaling, the crossing events have an exponentially small probability of order $O(e^{-c^2 t/2})$ (as estimated by displacing two neighbors by $\delta x_j = ct$ and $\delta x_{j+1} = -ct$). Hence the neglect of (i) is justified with that scaling. In addition, neglecting the fluctuations $\delta \tilde{x}_j/\sqrt{t}$ of the variables $z_j = x_j/t$ in the prefactor in (25) is also legitimate with that scaling.

Returning to the *unscaled* displacements δx_j , we have already seen for $N = 2$ that their cumulants have nontrivial additional $O(1)$ contributions plus exponential corrections of $O(e^{-c^2 t/2})$ [see Eqs. (17)–(20)]. Thus there are interesting deviations due to (i) and (ii) to the independent Gaussian picture. We will discuss them in the following two sections, first neglecting (ii), which leads to an analogy with an equilibrium problem, and second performing a more accurate analysis of (ii).

The above considerations are exact at long time $c^2 t \gg 1$ for any N . For large N this corresponds to regime III as defined in the Introduction.

C. Analogy with the equilibrium one-dimensional one-component plasma (jellium)

In this section we make a comparison between the time-dependent problem of ranked diffusion, characterized by $P(\vec{x}, t)$ in Eq. (25), and the equilibrium problem of the jellium model in one dimension (variously called the one-dimensional one-component plasma). The jellium model in one dimension consists of N particles confined in a harmonic potential and repelling each other via a pairwise Coulomb interaction (which is linear in one dimension). The energy function can be written as [11,12]

$$E[\vec{y}] = \frac{N^2}{2} \sum_i y_i^2 - \alpha N \sum_{i \neq j} |y_i - y_j|, \quad (28)$$

where y_i 's are assumed to be of $O(1)$. The first term describes the potential energy, while the second term describes the interaction energy. Here α is the strength of the interaction and is a dimensionless parameter. The system is supposed to be at equilibrium at temperature T_{eq} and the stationary probability distribution of the positions of the particles is given by the Gibbs-Boltzmann form

$$P_J[\vec{y}] = \frac{1}{Z_N} e^{-E[\vec{y}]/k_B T_{\text{eq}}}, \quad (29)$$

where k_B is the Boltzmann constant and Z_N is the normalizing partition function. In Eq. (29), the subscript J refers to the jellium model. We henceforth set $k_B T_{\text{eq}} = 1$ for convenience. It turns out to be convenient to rewrite the energy in Eq. (28) in terms of the ordered coordinates $y_1 < y_2 < \dots < y_N$. In terms of these ordered coordinates, using the identity in Eq. (24), we get

$$E[\vec{y}] = \frac{N^2}{2} \sum_{i=1}^N \left(y_i - \frac{2\alpha}{N} (2i - N - 1) \right)^2 - C_N(\alpha), \quad (30)$$

where the constant $C_N(\alpha)$ is given by

$$C_N(\alpha) = 2\alpha^2 \sum_{i=1}^N (2i - N - 1)^2 = \frac{2\alpha^2}{3} N^3 - \frac{2}{3} \alpha^2 N. \quad (31)$$

This implies that, in the ordered sector, the probability distribution of the y_i 's can be written as

$$P_J[\vec{y}] = \frac{1}{\tilde{Z}_N} \exp\left[-\frac{N^2}{2} \sum_{i=1}^N \left(y_i - \frac{2\alpha}{N} (2i - N - 1) \right)^2\right] \quad \text{for } y_1 < y_2 < \dots < y_N, \quad (32)$$

where \tilde{Z}_N is a normalization constant. The distribution has a maximum when y_i 's occupy the equidistant crystal positions, i.e.,

$$y_i^* = \frac{2\alpha}{N} (2i - N - 1). \quad (33)$$

The separation between successive particles is thus $4\alpha/N$. Defining the equilibrium density (normalized to unity) as

$$\rho_J(y) = \frac{1}{N} \sum_{i=1}^N \langle \delta(y - y_i) \rangle, \quad (34)$$

where $\langle \dots \rangle$ denotes an average over the equilibrium measure in Eq. (32). Using Eq. (33), we see that in the one-dimensional jellium model at equilibrium, the density in the large- N limit converges to a flat distribution supported over $[-2\alpha, +2\alpha]$, i.e.,

$$\rho_J(y) \approx \frac{1}{4\alpha} \mathbb{1}_{[-2\alpha, +2\alpha]}(y), \quad (35)$$

where the indicator function $\mathbb{1}_{[-2\alpha, +2\alpha]}(y)$ is 1 for $y \in [-2\alpha, +2\alpha]$ and is 0 outside. From Eq. (32) one can also infer the statistics of the positions of the particles in the gas in the two opposite limits: (i) noninteracting limit $\alpha \rightarrow 0$ and (ii) the strongly interacting limit $\alpha \rightarrow \infty$. In case (i), the particles are essentially independent, each having Gaussian fluctuations around the origin, with width $1/N$. In case (ii) the particles are localized at the crystal positions in Eq. (33), namely, $y_i^* = \frac{2\alpha}{N}(2i - N - 1)$, and around each position, the fluctuations are again Gaussian and independent with width $1/N$. The crossover between the two cases occurs for $\alpha = O(1)$, where the correlations are nontrivial.

In order to compare this equilibrium problem with the dynamics of ranked diffusion discussed earlier, we consider the asymptotic form of the probability distribution $P(\vec{x}, t)$ obtained in Eq. (25). As discussed at the end of the preceding section, a meaningful first approximation is to neglect the double product prefactor in Eq. (25) while retaining the ordering condition (hence accounting for particle crossing). The additional effect of this prefactor will be discussed in the following section. If we do so we obtain

$$P(\vec{x}, t) \propto \exp\left(-\frac{t}{4} \sum_{j=1}^N [z_j - c(2j - N - 1)]^2\right) \quad \text{for } z_1 < z_2 < \dots < z_N. \quad (36)$$

We are now ready to compare Eqs. (32) and (36). We see that the two probability distributions are formally equivalent provided we identify

$$z_i = \sqrt{\frac{2}{t}} N y_i, \quad \alpha = \frac{c\sqrt{t}}{2\sqrt{2}}, \quad (37)$$

which also gives $x_i = z_i t = \sqrt{2t} N y_i$. Since our original long-time formula (25) was obtained for $c^2 t \gg 1$ we see that the predictions from the equilibrium problem can be translated to the dynamics problem *a priori* only for $\alpha \gg 1$. However, it is interesting to present and use below some of the known results for the equilibrium problem at arbitrary α [with the idea that they may capture some of the effects of particle crossing for $c^2 t = O(1)$].

The above considerations, as well as the correspondence (37), hold for any N . Let us now consider the case where $N \gg 1$. In that case, from the average density in the equilibrium problem in Eq. (35) and using (37), we can make a prediction for the density of the z_i variables [defined similarly to (34)] in

the dynamics problem, namely,

$$\rho(z) \approx \frac{1}{2cN} \mathbb{1}_{[-cN, +cN]}(z). \quad (38)$$

The prediction for the density in the original coordinates of the particles, $x_i = t z_i$, thus takes the form

$$\rho(x, t) \approx \frac{1}{2cNt} \mathbb{1}_{[-cNt, +cNt]}(x). \quad (39)$$

This describes the dynamics of a gas whose two edges move ballistically with constant speed cN , describing two light cones that bound the trajectories of the gas particles [see Fig. 1(c')]. The prediction (39) is in agreement with the density computed numerically and represented in Fig. 1(c''). It corresponds to regime III discussed there.

Let us now recall for completeness some exact results for various observables that were derived recently for the jellium model for any α and later consider the large- α limit where it leads to predictions for the ranked diffusion at long time. Consider now the gap between two consecutive particles both in the bulk and at the edges. Consider the jellium model in Eq. (32) and let $g_i = y_{i+1} - y_i$ define the spacing between the i th and $(i+1)$ th particles of the jellium gas at equilibrium. First, we consider the midgap, i.e., setting $i = N/2$ (this corresponds to the typical gap in the bulk). In this case, the distribution of the midgap, in the large- N but fixed- α limit, takes the scaling form [13]

$$\begin{aligned} \mathcal{P}_{\text{mid gap}}(g, N) &\sim N H_\alpha(gN), \\ H_\alpha(z) &= \theta(z) [A(\alpha)]^2 \int_{-\infty}^{\infty} dy e^{-[(y+z-4\alpha)^2 + y^2]/2} \\ &\quad \times F_\alpha(y + 4\alpha) F_\alpha(-y - z + 8\alpha), \end{aligned} \quad (40)$$

where the function $F_\alpha(x)$ satisfies the nonlocal differential equation

$$\frac{dF_\alpha(x)}{dx} = A(\alpha) F_\alpha(x + 4\alpha) e^{-x^2/2}, \quad (41)$$

with the boundary conditions $F_\alpha(x \rightarrow +\infty) = 1$ and $F_\alpha(x \rightarrow -\infty) = 0$. This equation can be thought of as an eigenvalue equation, with $A(\alpha)$ the unique eigenvalue for which there exists a solution that satisfies both boundary conditions. In particular, for α large, it behaves as $A(\alpha \rightarrow \infty) \sim 1/\sqrt{2\pi}$ [6,10]. This function $F_\alpha(x)$ often appears in the context of one-dimensional one-component plasma [10,11,13] (see also [6]) and it has the following asymptotic behaviors [10,11]:

$$F_\alpha(x) \sim 1 - e^{-x^2/2 + \alpha(x^2)} \quad \text{for } x \rightarrow \infty, \quad (42)$$

$$F_\alpha(x) \sim e^{-|x|^3/24\alpha + \alpha(x^3)} \quad \text{for } x \rightarrow -\infty. \quad (43)$$

Let us now focus on the distribution in Eq. (40) in the large- α limit. In this limit we can approximate the integral over y in Eq. (40) by a saddle-point method. The minimum of the argument in the exponential function occurs at $y^* = (4\alpha - z)/2$. At this value of y , the F_α functions in the integrand in Eq. (40) read $[F_\alpha(6\alpha - z/2)]^2$. Since α is large, this factor essentially contributes unity, using Eq. (42), as long as $z < 12\alpha$. We will see in the following that indeed this is true in the range of z where the gap distribution has a peak. Therefore, the saddle-point analysis gives, up to a multiplicative

prefactor,

$$\lim_{\alpha \rightarrow \infty} H_\alpha(z) \sim e^{-(1/4)(z-4\alpha)^2}. \quad (44)$$

Hence, the distribution of the midgap, in the limit of large α , approaches a Gaussian distribution

$$\mathcal{P}_{\text{mid gap}}(g) \sim e^{-(N^2/4)(g-4\alpha/N)^2}, \quad (45)$$

with mean at $g = 4\alpha/N$ and variance $2/N^2$. Thus, in this limit of large α (and large N), one can express the random variable $g_{\text{mid gap}}$ (i.e., the midgap) as

$$g_{\text{mid gap}} \approx \frac{4\alpha}{N} + \frac{\sqrt{2}}{N} \mathcal{N}(0, 1), \quad (46)$$

where $\mathcal{N}(0, 1)$ is a standard normal variable with zero mean and unit variance. We can now use this result and the correspondence in Eq. (37) to predict the distribution of the midgap $g_{\text{mid gap}}^{\text{RD}}$ in the dynamics problem of ranked diffusion (the superscript RD refers to ranked diffusion). We get

$$\begin{aligned} g_{\text{mid gap}}^{\text{RD}} &= z_{N/2+1} - z_{N/2} \approx \sqrt{\frac{2}{t}} N \left(\frac{4\alpha}{N} + \frac{\sqrt{2}}{N} \mathcal{N}(0, 1) \right) \\ &= 2c + \frac{2}{\sqrt{t}} \mathcal{N}(0, 1). \end{aligned} \quad (47)$$

Returning to the original $x_i = t z_i$ coordinates, we finally get the midgap distribution as

$$\begin{aligned} G_{\text{mid gap}}^{\text{RD}} &= x_{N/2+1}(t) - x_{N/2}(t) \\ &= t g_{\text{mid gap}}^{\text{RD}} \approx 2ct + 2\sqrt{t} \mathcal{N}(0, 1). \end{aligned} \quad (48)$$

The same result holds for all the gaps inside the bulk of the jellium model [13] and hence equivalently for the ranked diffusion model. However, the behavior of the gap distribution changes as one approaches the edges of the jellium model, i.e., $g_{\text{edge gap}} = y_N - y_{N-1}$, which has the distribution in the large- N limit [11]

$$\mathcal{P}_{\text{edge gap}}(g) \sim N h_\alpha(gN), \quad (49)$$

$$h_\alpha(z) = \theta(z) [A(\alpha)]^2 \int_{-\infty}^{\infty} dy e^{-[(y+z-4\alpha)^2 + y^2]^{1/2}} F_\alpha(y + 4\alpha), \quad (50)$$

where $F_\alpha(x)$ is the same function as defined in Eq. (41). Once again, to make a correspondence to the ranked diffusion problem, we need to consider the limit of α large. In that limit, one can again approximate this integral (50) by the saddle-point method. Following exactly the same argument as in the midgap case, one gets

$$\lim_{\alpha \rightarrow \infty} h_\alpha(z) \sim \frac{1}{\sqrt{4\pi}} e^{-(1/4)(z-4\alpha)^2}. \quad (51)$$

Hence, using (49), we again get a Gaussian distribution for the edge gap in the jellium model in the large- α limit

$$\mathcal{P}_{\text{edge gap}}(g) \sim e^{-(N^2/4)(g-4\alpha/N)^2}. \quad (52)$$

Thus, in the large- α limit, the edge and bulk gaps in the jellium model behave in the same way, namely,

$$g_{\text{edge gap}} \approx \frac{4\alpha}{N} + \frac{\sqrt{2}}{N} \mathcal{N}(0, 1). \quad (53)$$

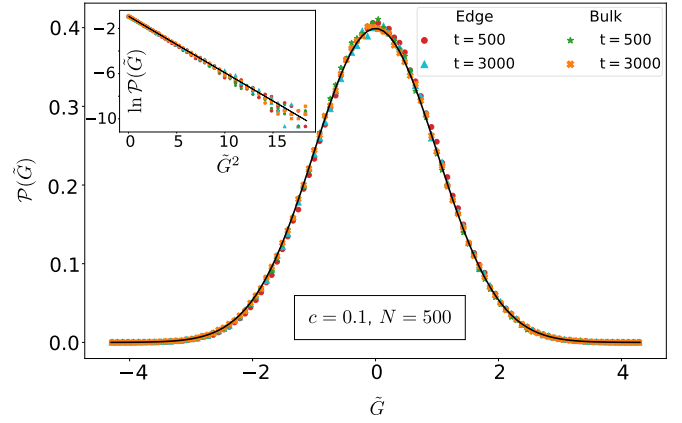


FIG. 4. Plot of the distribution of the centered and scaled gap $\tilde{G} = \frac{G^{\text{RD}} - 2ct}{2\sqrt{t}}$ for times $t = 500$ and 3000 , from the numerical simulation of the Langevin equation (4) for both the midgap $G^{\text{RD}} \equiv G_{\text{mid gap}}^{\text{RD}}$ and the edge gap $G^{\text{RD}} \equiv G_{\text{edge gap}}^{\text{RD}}$. Here $N = 500$ and $c = 0.1$ (note that $c^2 t$ is the dimensionless time). Shown for comparison is the normal Gaussian distribution $e^{-x^2/2}/\sqrt{2\pi}$ as predicted in (48) and (54) (black solid line). The inset shows $\ln \mathcal{P}$ as a function of \tilde{G}^2 using the same numerical data. The black solid line is the normal Gaussian distribution.

Correspondingly, the edge gap and in the midgap behave in a same way, namely,

$$G_{\text{edge gap}}^{\text{RD}} = x_N(t) - x_{N-1}(t) \approx 2ct + 2\sqrt{t} \mathcal{N}(0, 1). \quad (54)$$

Although this result, together with (48), was obtained here at large N , we note that, by comparing it to Eq. (18), it already holds for $N = 2$ for the first two cumulants, which thus appears to be independent of N .

In summary, the predictions (48) and (54) from the analogy with the equilibrium are in agreement with the discussion at the end of the preceding section, i.e., that on the scale $\delta x_i \sim \sqrt{t}$ the fluctuations are independently Gaussian, as indeed recovered in the large- α limit of the jellium. In Fig. 4 we verify by Monte Carlo simulations the two analytical predictions for the gaps in the ranked diffusion model in Eqs. (48) and (54), respectively. We see that the agreement is indeed excellent if the gaps are scaled by \sqrt{t} .

However, this is not the end of the story for the dynamics problem, and in the next section we will compute the higher cumulants of the particle positions x_i at long time, which exhibit deviations from this leading Gaussian behavior.

D. More accurate treatment of the long-time limit: Higher cumulants

In this section we return to the complete asymptotic form for the joint PDF at long time (23) and (25) and we obtain all the cumulants of the particle positions x_i to $O(1)$ accuracy.

I. Case $N = 2$

Let us start with $N = 2$ for simplicity. Consider the long-time asymptotic formula (16). Let us recall that the original variable is $y = x_2 - x_1 = zt$. We can consider the sector $y > 0$: Indeed, we will use a saddle-point method, and there will be one saddle point inside each sector and the result will not

depend on the sector (discussed below). We want to evaluate the cumulant generating function

$$\langle e^{\lambda y} \rangle = \langle e^{t\lambda z} \rangle \simeq \int_0^{+\infty} dz \exp \left[-\frac{t}{4}(z - 2c)^2 + \ln \left(\frac{z}{z + 2c} \right) + f(t) + t\lambda z \right], \quad (55)$$

where we have inserted (16) and the normalization factor $f(t) = -\ln(2\sqrt{2\pi t})$ is immaterial for the following. At long t there is a unique saddle point at $z = z^* = 2c + 2\lambda$. We require that $2c + 2\lambda > 0$ (in fact for the cumulants we only need λ in the neighborhood of $\lambda = 0$). From the saddle-point method we thus obtain

$$\langle e^{\lambda y} \rangle \simeq \exp \left[2t\lambda + 2\lambda^2 t + \ln \left(\frac{2c + 2\lambda}{2c + \lambda} \right) \right], \quad (56)$$

where we have fixed the normalization so that the right-hand side is equal to unity at $\lambda = 0$. Using that $\ln \langle e^{\lambda y} \rangle = \sum_{k \geq 1} \frac{\lambda^k}{k!} \langle y^k \rangle_c$ and expanding in λ , we obtain all the cumulants. This reproduces the results in Eqs. (17)–(20) up to and including $O(1)$ terms at long time and gives the more general formula for $k \geq 2$,

$$\langle y^k \rangle_c = \frac{1}{c^k} (-1)^{k-1} (k-1)! (2^k - 1) + o(1). \quad (57)$$

Several remarks are in order. First, since (16) depends only on $|z|$, instead of choosing the sector $y > 0$ we could have

done the exact same calculation replacing y by $|y|$ and z by $|z|$. The saddle point is then at $|z| = 2c + 2\lambda$, so there are in fact two identical saddle points for each sign of y . Hence, to the same accuracy, $\langle (|y| - 2ct)^k \rangle_c = \langle y^k \rangle_c$ given by (57). Next we see that (56) holds for any $\lambda > -c$, but fails when $\lambda \leq -c$, since for $\lambda = -c$ the saddle point reaches $z = 0$. The average $\langle e^{\lambda y} \rangle$ is then dominated by the vicinity of $z = 0$, i.e., by events which involve particle crossings, and the two sectors cannot be neatly separated. Finally, we know from the exact results (17)–(20) that the $o(1)$ corrections in (57) should be exponentially small $O(e^{-c^2 t/2})$ at long time. However, the above saddle-point method, if pushed to next order, will lead to a power law in time corrections $O(1/t^k)$. This apparent paradox is resolved in Appendix B, where it is shown that (56) has indeed only exponentially small corrections in time. The reason for that is that (16) itself comes from a first saddle-point method, and both saddle points should be considered simultaneously. In Appendix B we identify these exponentially small corrections to (56) to come precisely from particle crossing, which are exponentially rare for $c^2 t \gg 1$.

2. Case of arbitrary N

Let us now turn to arbitrary N and consider the sector $x_1 < x_2 < \dots < x_N$, recalling that we define $x_j = tz_j$. Let us compute the generating function at long time, inserting the asymptotic form (25),

$$\begin{aligned} \left\langle \exp \left(\sum_j \lambda_j x_j \right) \right\rangle &= \left\langle \exp \left(t \sum_j \lambda_j z_j \right) \right\rangle \\ &\simeq \int_{z_1 < z_2 < \dots < z_N} dz_1 \cdots dz_N \exp \left(-\frac{t}{4} \sum_{j=1}^N [z_j - c(2j - N - 1)]^2 + t \sum_{j=1}^N \lambda_j z_j \right. \\ &\quad \left. + \sum_{1 \leq a < b \leq N} \ln \frac{z_b - z_a}{z_b - z_a + 2c} + f(t) \right), \end{aligned} \quad (58)$$

where again $f(t)$ is an unimportant normalization. In this sector there is a unique saddle point at long t given by

$$z_j = z_j^* = c(2j - N - 1) + 2\lambda_j, \quad j = 1, \dots, N. \quad (59)$$

We will assume that the z_j^* are in the sector considered, i.e., that all $c(2j - N - 1) + 2\lambda_j > 0$ for $j = 1, \dots, N$, which is certainly the case when the λ_j are all in a neighborhood of zero. Then the saddle-point method gives

$$\left\langle \exp \left(\sum_j \lambda_j x_j \right) \right\rangle \simeq N! \exp \left[\sum_{j=1}^N c(2j - N - 1)t\lambda_j + t \sum_{j=1}^N \lambda_j^2 + \sum_{1 \leq a < b \leq N} \ln \left(\frac{c(b-a) + \lambda_b - \lambda_a}{c + (b-a)c + \lambda_b - \lambda_a} \right) \right], \quad (60)$$

where we used $\sum_{1 \leq a < b \leq N} \frac{b-a}{1+b-a} = 1/N!$ to normalize the formula.

Upon expanding the logarithm of (60) in the parameters λ_j , we can now compute all the joint cumulants of the deviations from the perfect crystal, defined as $\delta x_j = x_j - c(2j - N - 1)t$. First, we note that the double sum in (60) involves only pairs of distinct variables λ_j . Hence the cumulants involving more than two particles are zero, e.g.,

$$\langle \delta x_i \delta x_j \delta x_k \rangle_c = 0 \quad \text{for } i < j < k. \quad (61)$$

To compute the only nonzero cumulants (i.e., involving only one or two particles) we first define the function

$$f_k(x) = \ln \left(\frac{ck + x}{c + ck + x} \right), \quad (62)$$

which has derivatives

$$c^k f_k^{(n)}(0) = (-1)^{n-1} (n-1)! \left(\frac{1}{k^n} - \frac{1}{(k+1)^n} \right). \quad (63)$$

From the logarithm of (60) we obtain the single-particle cumulants as

$$\langle (\delta x_i)^n \rangle_c = \sum_{i < j \leq N} \partial_{\lambda_i}^n f_{j-i}(\lambda_j - \lambda_i)|_{\lambda_i=\lambda_j=0} + \sum_{1 \leq j < i} \partial_{\lambda_i}^n f_{i-j}(\lambda_i - \lambda_j)|_{\lambda_i=\lambda_j=0} + 2t \delta_{n,2} \quad (64)$$

$$= \sum_{i < j \leq N} (-1)^n f_{j-i}^{(n)}(0) + \sum_{1 \leq j < i} f_{i-j}^{(n)}(0) + 2t \delta_{n,2}. \quad (65)$$

This leads to, for $1 \leq i \leq N$ and $n \geq 2$,

$$\langle (\delta x_i)^n \rangle_c = \frac{1}{c^n} (n-1)! \left[\frac{1}{(N-i+1)^n} - 1 + (-1)^{n-1} \left(1 - \frac{1}{i^n} \right) \right] + 2t \delta_{n,2}. \quad (66)$$

We see that at large N , for $i = O(1)$, i.e., at the left edge of the gas, one has

$$\lim_{N \rightarrow +\infty, i=O(1)} \langle (\delta x_i)^n \rangle_c = \frac{1}{c^n} (n-1)! \left(-2\delta_{n,\text{even}} + \frac{(-1)^n}{i^n} \right) + 2t \delta_{n,2}. \quad (67)$$

We see that in the bulk of the gas, i.e., for $i \rightarrow +\infty$, the odd cumulants decay to zero, while the even cumulants $n \geq 4$ decay from $-\frac{3}{c^n}(n-1)!$ for $i = 1$, to a finite limit $-\frac{2}{c^n}(n-1)!$, which is uniform over the bulk of the gas. Hence the fluctuations are slightly larger near the edge but remain finite in the bulk. On the right edge the result is similar, with the term $\frac{(-1)^n}{i^n}$ replaced by $\frac{1}{(N-i+1)^n}$.

Next we compute the cumulants involving two particles (for $j > i$, $m, n \geq 1$, and $N \geq 2$). We find

$$\begin{aligned} \langle \delta x_i^n \delta x_j^m \rangle_c &= \partial_{\lambda_i}^n \partial_{\lambda_j}^m f_{j-i}(\lambda_j - \lambda_i)|_{\lambda_i=\lambda_j=0} = (-1)^n f_{j-i}^{(n+m)}(0) \\ &= \frac{1}{c^n} (-1)^{m-1} (n+m-1)! \left(\frac{1}{(j-i)^{n+m}} - \frac{1}{(j-i+1)^{n+m}} \right). \end{aligned} \quad (68)$$

We note that these correlations are independent of N and decay quickly to zero as a function of the distance between the two particles.

These formulas are exact for all N . For concreteness, let us display some of the predictions for $N = 2, 3$. For simplicity, we set here $c = 1$. For $N = 2$ this gives

$$\langle (\delta x_1)^2 \rangle_c = \langle (\delta x_2)^2 \rangle_c = 2t - \frac{3}{4}, \quad \langle \delta x_1 \delta x_2 \rangle_c = \frac{3}{4}, \quad (69)$$

$$\langle (\delta x_1)^3 \rangle_c = -\langle (\delta x_2)^3 \rangle_c = -\frac{7}{4}, \quad \langle \delta x_1 (\delta x_2)^2 \rangle_c = -\langle (\delta x_1)^2 \delta x_2 \rangle_c = -\frac{7}{4}. \quad (70)$$

For $N = 3$ we obtain

$$\langle \delta x_1 \rangle = -\frac{2}{3}, \quad \langle \delta x_2 \rangle = 0, \quad \langle \delta x_3 \rangle_c = \frac{2}{3}, \quad (71)$$

$$\langle \delta x_1^2 \rangle_c = \langle \delta x_3^2 \rangle_c = 2t - \frac{8}{9}, \quad \langle \delta x_2^2 \rangle_c = 2t - \frac{3}{2}, \quad \langle \delta x_1 \delta x_2 \rangle_c = \langle \delta x_2 \delta x_3 \rangle_c = \frac{3}{4}, \quad \langle \delta x_1 \delta x_3 \rangle_c = \frac{5}{36}, \quad (72)$$

$$\langle \delta x_1^3 \rangle_c = -\langle \delta x_3^3 \rangle_c = -\frac{52}{27}, \quad \langle \delta x_2^3 \rangle_c = 0, \quad \langle \delta x_1 \delta x_2^2 \rangle_c = -\langle \delta x_1^2 \delta x_2 \rangle_c = -\frac{7}{4}, \quad (73)$$

$$\langle \delta x_1^2 \delta x_3 \rangle_c = -\langle \delta x_1 \delta x_3^2 \rangle_c = \frac{19}{108}, \quad \langle \delta x_2 \delta x_3^2 \rangle_c = -\langle \delta x_2^2 \delta x_3 \rangle_c = -\frac{7}{4}, \quad \langle \delta x_1 \delta x_2 \delta x_3 \rangle_c = 0. \quad (74)$$

Next one can use these formula to compute the cumulants of the relative distance between any two particles. Since the cumulants of x_j and of δx_j are by definition identical, we will simply use the particle positions x_j here. For $1 \leq i < j \leq N$ one finds

$$\langle (x_j - x_i)^n \rangle_c = \frac{(n-1)!}{c^n} \{ i^{-n} + (-1)^n (2^n - 2) [(-i+j+1)^{-n} - (j-i)^{-n}] \} \quad (75)$$

$$+ (-1)^n (-i+N+1)^{-n} + (-1)^n j^{-n} + (-j+N+1)^{-n} - 2(-1)^n - 2 + 4t \delta_{n,2} + 2tc(j-i) \delta_{n,1}, \quad (76)$$

which for $j = i+1$ gives the cumulants of the gaps, for which one finds, for $1 \leq i \leq N-1$,

$$\begin{aligned} \langle (x_{i+1} - x_i)^n \rangle_c &= \frac{(n-1)!}{c^n} [i^{-n} + (N-i)^{-n} + (-1)^n (-i+N+1)^{-n} + (-1)^n (i+1)^{-n} \\ &\quad + (-1)^n (-2^{1-n} - 2^n + 1) - 2] + 4t \delta_{n,2} + 2ct \delta_{n,1}. \end{aligned} \quad (77)$$

Again, in the large- N limit one finds some distinct behavior at the two edges and that the cumulants of the gap reach a finite limit inside the bulk given by the second line of (77).

Similarly, one finds that the cumulants of the total size of the gas (i.e., its span) are given by

$$\langle (x_N - x_1)^n \rangle_c = (-1)^n \frac{(n-1)!}{c^n} [2^n N^{-n} - (2^n - 2)(N-1)^{-n} + 2] + 4t\delta_{n,2} + 2c(N-1)t\delta_{n,1}. \tag{78}$$

For large N the n th cumulant ($n > 1$) of the total size of the gas converge quickly to some finite limit

$$\langle (x_N - x_1)^n \rangle_c \simeq 2(-1)^{n-1} \frac{(n-1)!}{c^n} \left(1 - \frac{1}{N^n} + \dots \right) + 4t\delta_{n,2} + 2c(N-1)t\delta_{n,1}, \tag{79}$$

which, at large N , is equivalent to the sum of independent fluctuations, $\langle (\delta x_N)^n \rangle_c + (-1)^n \langle (\delta x_1)^n \rangle_c$, since the mutual fluctuations decay at large distance, as pointed out above. It is interesting that there are non-Gaussian persistent correlations at long time, on the scale of the gas, even at large N .

To summarize, we have obtained a complete quantitative picture of the $O(1)$ fluctuations at long time in the expanding crystal which goes beyond the independent Gaussian $O(\sqrt{t})$ fluctuations discussed in the previous sections. These result are valid for $c^2 t \gg 1$ and any N . From the considerations for $N = 2$ (see Appendix A), we can surmise that the corrections to these cumulants, as well as to (60), are exponentially small at long time and related to particle crossing (hence also in part to the finite- α physics of the equilibrium jellium).

IV. APPROACH VIA THE BURGERS EQUATION

Until now we have focused on taking the long-time limit first, with a fixed number of particles N . In this section we first recall the exact hydrodynamic equation which describes the evolution of the density. Using this equation, we then study the limit of large N first, at arbitrary fixed time t . This provides a description of the dense regimes I and II discussed in the Introduction. Finally, we compare the predictions with numerical simulations.

A. Burgers equation and large- N limit

Let us first recall the general approach developed in [18]. Let us consider again the Langevin equation (4) for N particles. One defines the density field $\rho(x, t)$ and the rank field $r(x, t)$ as

$$\begin{aligned} \rho(x, t) &= \frac{1}{N} \sum_i \delta(x - x_i(t)) = \partial_x r(x, t), \\ r(x, t) &= \int_{-\infty}^x dx' \rho(x', t) - \frac{1}{2}, \end{aligned} \tag{80}$$

respectively. It is convenient to choose the rank field $r(x, t)$ increasing monotonically from $-\frac{1}{2}$ at $x = -\infty$ to $+\frac{1}{2}$ at $x = +\infty$. Then it is shown in [18], using the Dean-Kawasaki method [23–25], that the rank field satisfies the stochastic equation

$$\begin{aligned} \partial_t r(x, t) &= T \partial_x^2 r(x, t) - 2Ncr(x, t) \partial_x r(x, t) \\ &+ \frac{1}{\sqrt{N}} \sqrt{2T \partial_x r(x, t)} \eta(x, t). \end{aligned} \tag{81}$$

The first term on the right-hand side of (81) originates from diffusion, the second is a convection term where the local velocity is proportional to the local rank, and the third term is the noise, originating from local Brownian dynamics. In

[18] the case of an additional external potential $V(x)$ was also considered, but here we set it to zero. Hence Eq. (81) is the Burgers equation with a multiplicative noise. Note that the function $r(x, t)$ is constrained to be increasing in x , so the density remains positive. This equation is formally exact for arbitrary N [with the possible mathematical caveat that $r(x, t)$ is a discontinuous stochastic function]. Here we recall that we consider $c > 0$.

Let us now discuss the large- N limit. As discussed in [18], there are *a priori* two natural scalings of c in that limit. In both cases, the noise term is formally subdominant.

B. Detailed solution for $c = \gamma/N$ and comparison with numerics

(i) The first choice is to keep c fixed. In that case, one defines a rescaled time $\tau = Nt$. The noise term and the diffusion term both become $O(1/N)$ and (81) simply becomes the inviscid Burgers equation $\partial_\tau r = -2cr \partial_x r$. The solution is obtained implicitly by solving for $r \equiv r(x, t)$ equation [18]

$$r = r_0(x - 2c\tau), \tag{82}$$

where $r(x, 0) = r_0(x)$ is the initial condition. Since $c > 0$ there is a unique solution with no shocks. An example is the square density initial condition ($\ell > 0$)

$$\rho(x, t) = \frac{1}{2(\ell + c\tau)} \theta(\ell + c\tau - |x|), \quad \tau = Nt, \tag{83}$$

which shows that the repulsive gas expands linearly in time with sharp edges at $\pm c\tau = \pm cNt$. This result (restoring $\tau = Nt$) matches with the prediction (39) which was obtained in the long-time limit followed by the large- N limit. Note that here the convergence to the form (83) occurs quite fast, on a timescale $\tau = O(1)$, that is, $t \sim 1/N$. Comparing with the discussion in the Introduction, we see that this time regime corresponds to regime II, where the square density forms and expands, and in the inviscid Burgers equation the edges are sharp on the scale $x = O(1)$.

(ii) Here we will consider the second and richer choice of scaling, i.e., $c = \gamma/N$ where $\gamma > 0$ is fixed. In that case, only the noise term is subdominant $O(1/\sqrt{N})$ in (81), and one obtains the viscous Burgers equation in the original time variable t , namely,

$$\partial_t r(x, t) = T \partial_x^2 r(x, t) - 2\gamma r(x, t) \partial_x r(x, t). \tag{84}$$

As we will see below, the solution of this equation with a square density initial condition (with $\ell > 0$) is similar in the bulk to (83), since the first term on the right-hand side of (84) is essentially zero for a flat density profile. This also leads to an expansion of the gas which is linear in time with the same speed. The main difference occurs near the edges, the sharp edges of (81) at $\pm \gamma t = \pm cNt$ being replaced by a smooth

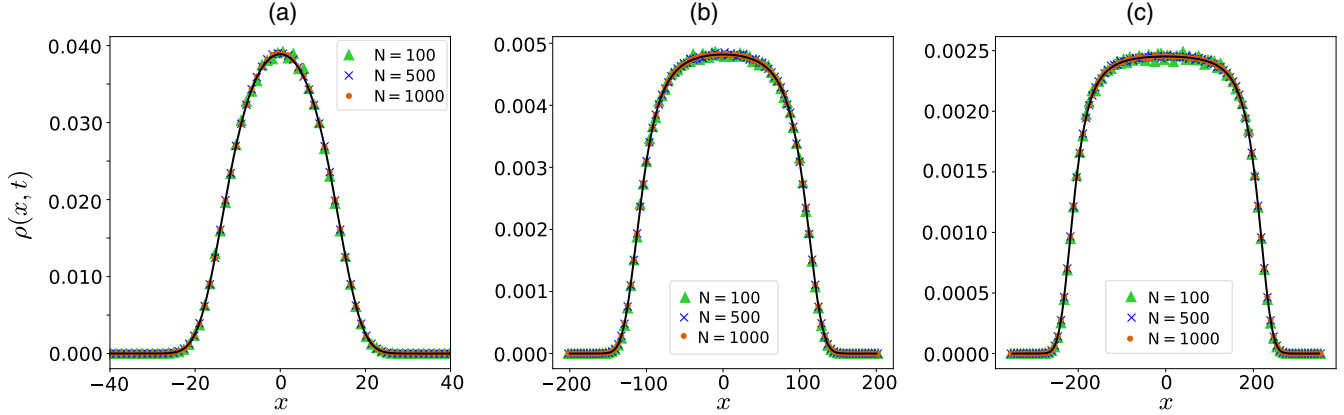


FIG. 5. Plot of the density $\rho(x, t)$ evaluated numerically from the Langevin equation, at three different times (a) $t = 10$, (b) $t = 100$, and (c) $t = 200$ for $\gamma = 1$ and $T = 1$. The initial condition is that all particles are at the origin at time zero. For each time we simulated the density profile for three different combinations of N and c with fixed $\gamma = Nc = 1$. The averaging is done over 10^4 realizations of the noise. The numerical data are compared with the analytical prediction with a δ -function initial condition from Eq. (87) (black solid lines).

profile with a boundary layer form. For attractive interactions studied in [18] there is a stationary state and the boundary layer has a width $\xi = \frac{T}{cN} = \frac{T}{\gamma}$ determined by comparing the two terms on the right-hand side of (84). It turns out that in the case studied here, i.e., repulsive interactions and a δ initial condition for the density, the gas is always far from stationarity and we show below that the scale which determines the size of the boundary layer is the diffusion length scale $\ell_T = \sqrt{2Tt}$ [within the boundary layers the three terms in (84) are of the same order].

Note that the characteristic length scale and timescale associated with the Burgers equation (84) are $x \sim T/\gamma = T/Nc$ and $t \sim T/\gamma^2 = T/N^2c^2 = t_1^*$, respectively [which would allow us to eliminate the γ dependence in (84)]. Hence this equation naturally describes the crossover between regimes I and II.

In order to compare with the numerics we give here the explicit form of the density and rank field obtained by solving analytically Eq. (84) for two cases.

(i) For the initial condition corresponding to all particles initially at $x = 0$, as in (9), which corresponds to $r_0(x) = \frac{1}{2}\text{sgn}(x)$, one finds [e.g., using Eq. (25) in [18]]

$$r(x, t) = -\frac{T}{\gamma} \partial_x \ln[f(x, t) + f(-x, t)], \quad (85)$$

$$\begin{aligned} f(x, t) &= \int_0^{+\infty} \frac{dw}{\sqrt{4\pi Tt}} \exp\left(-\frac{(w-x)^2}{4Tt} - \frac{\gamma w}{T}\right) \\ &= \frac{1}{2} \exp\left(\frac{1}{4T}\gamma(\gamma t - 2x)\right) \text{erfc}\left(\frac{\gamma t - x}{2\sqrt{Tt}}\right). \end{aligned} \quad (86)$$

This leads to the time-dependent density

$$\rho(x, t) = \partial_x r(x, t) = \frac{e^{-(x-\gamma t)^2/4tT} \left[\frac{e^{\gamma x/T} \text{erfc}\left(\frac{\gamma t+x}{2\sqrt{Tt}}\right)}{\sqrt{t}\sqrt{T}} + \text{erfc}\left(\frac{\gamma t-x}{2\sqrt{Tt}}\right) \left(\frac{1}{\sqrt{t}\sqrt{T}} - \frac{\sqrt{\pi}\gamma e^{(\gamma t+x)^2/4tT} \text{erfc}\left(\frac{\gamma t+x}{2\sqrt{Tt}}\right)}{T} \right) \right]}{\sqrt{\pi} \left[\text{erfc}\left(\frac{\gamma t-x}{2\sqrt{Tt}}\right) + e^{\gamma x/T} \text{erfc}\left(\frac{\gamma t+x}{2\sqrt{Tt}}\right) \right]^2}. \quad (87)$$

(ii) For a box shape initial density of width 2ℓ , i.e., $\rho(x, 0) = \frac{1}{2\ell}\theta(\ell - |x|)$, the solution is given by [see Eqs. (171) and (172) in [18]], where one sets $T = 1$,

$$\begin{aligned} \rho(x, t) &= \partial_x r(x, t), \\ r(x, t) &= -\frac{1}{\gamma} \partial_x \ln[f(x, t) + f(-x, t)], \quad (88) \\ f(x, t) &= \frac{e^{-\gamma x^2/4(\ell+\gamma t)}}{\sqrt{1+\frac{\gamma t}{\ell}}} \text{erf}\left(\frac{\ell+\gamma t+x}{2\sqrt{t}\sqrt{1+\frac{\gamma t}{\ell}}}\right) \\ &\quad + e^{\gamma(\ell+\gamma t+2x)/4} \text{erfc}\left(\frac{\ell+\gamma t+x}{2\sqrt{t}}\right). \end{aligned} \quad (89)$$

For $\ell \rightarrow 0$ this formula returns the result (88) for the δ initial condition.

The analytical formula (87) for the density, with a δ initial condition, is plotted in Fig. 5 for several values of t (solid line). We see that in the limit of long time $t \gg \frac{1}{\gamma^2}$ the density predicted by the Burgers equation evolves towards a flat profile for $x \in [-\gamma t, \gamma t]$. In addition, as can be seen in the figure, there is a boundary layer at each edge. From (87) one can derive the precise form of this boundary layer (see Appendix C) and one finds that the density near the right edge at $x = \gamma t$ takes the form

$$\begin{aligned} \rho(x, t) &= \frac{1}{\gamma t} \hat{\rho}\left(\frac{x - \gamma t}{\sqrt{Tt}}\right), \\ \hat{\rho}(y) &= \frac{e^{-y^2/2} [2 + \sqrt{\pi} e^{y^2/4} y \text{erfc}(-\frac{y}{2})]}{2\pi \text{erfc}(-\frac{y}{2})^2}. \end{aligned} \quad (90)$$

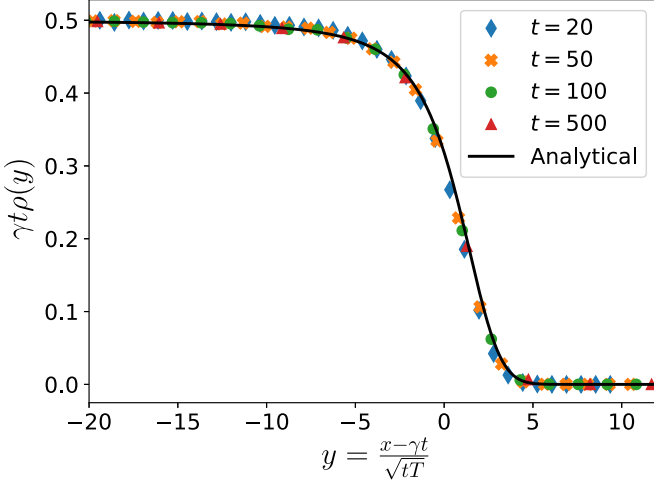


FIG. 6. Comparison of numerical simulation of the boundary layer at the right edge with the result from Eq. (90). In the simulation $\gamma = cN = 7$ with $N = 1000$, $c = 0.007$, and $T = 1$. We chose four different times $t \in \{20, 50, 100, 500\}$, which are inside regime II. The averaging is done over 10 000 realizations of the noise and at $t = 0$ all particles are at $x = 0$.

The characteristic width is thus the diffusion length $\ell_T = \sqrt{Tt}$ [see (1)]. As mentioned above, here $t = O(T/\gamma^2) = O(T/(cN)^2)$; hence this width is itself of order T/cN . The scaling function has the asymptotic behavior $\hat{\rho}(y) \simeq \frac{1}{2} - \frac{1}{y^2}$ for $y \rightarrow -\infty$, which thus matches the density of the plateau $\rho(x, t) \simeq \frac{1}{2\gamma t} = \frac{1}{2cNt}$. On the other side it has a fast decay, $\hat{\rho}(y) = \frac{y}{2\sqrt{\pi}} e^{-y^2/4}$ for $y \rightarrow +\infty$.

We have plotted the prediction (90) in Fig. 6 (solid line), where it is also compared with numerical simulations for various times inside regime II (discussed below). We see that the agreement of the data with the scaling function is excellent. In the opposite limit $t \ll \frac{1}{\gamma^2}$ one can check that the formula (87) converges to the Gaussian profile for independent diffusing particles $\rho(x, t) \simeq \frac{1}{\sqrt{4\pi Tt}} e^{-x^2/4Tt}$.

We now compare these predictions with a direct numerical calculation of the trajectories $x_j(t)$ from the Langevin equations (4), where we set $T = 1$ and $c = \gamma/N$. In Fig. 5 we study the case where all the particles start from the origin at $t = 0$. We plot the numerically evaluated density $\rho(x, t)$ as a function of x for different times t (and several values of N), averaged over 10^4 realizations of the noise. This is compared with the prediction in Eq. (87) with an initial δ -function density. We see that the agreement is quite good; hence in this time regime the density is very well described by the deterministic Burgers equation even for moderate values of N .

The matching between the solution derived from the Burgers equation and the numerical simulations can be further investigated by looking at the rank fields. In Fig. 7 we present the numerical evaluation of the rank fields for $N = 1000$ for both the square and the δ initial conditions for $t = 50$ and $\gamma = 2$. In the inset we have plotted the difference between the observed and predicted values of the rank field as a function of x , as given in (88) and (87). One can see that these differences are quite small.

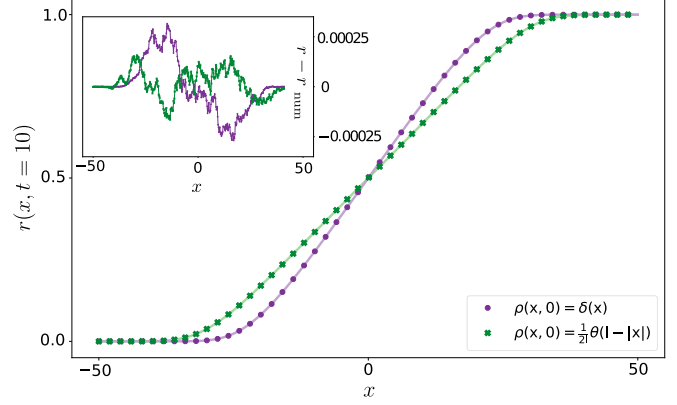


FIG. 7. Rank field $r(x, t)$ computed numerically (dots and crosses) and from the analytical expression (solid lines) for two different initial conditions. Green crosses represent the square initial condition $\rho(x, 0) = \frac{1}{2l}\theta(l - |x|)$ for $l = 10$. The numerical data are compared with the analytical expression (88) (green solid line connecting the crosses). The purple dots show the numerical data for the initial condition where all the particles start from the origin. The analytical expression (85) is represented by the purple solid line connecting the circles. The inset shows the pointwise difference between numerical data $r_{\text{num}}(x, t)$ and the analytical expression $r(x, t)$ for both δ and square initial conditions. The deviations are of order 10^{-3} . For both plots the rank field is measured at $t = 10$ with $\gamma = 2$, $T = 1$, and $N = 1000$. Here the data are averaged over 10^3 different realizations, which shows a small systematic deviation, due to the finite- N effects (see Fig. 8).

Next we study how these differences between the observed and the predicted values of the rank field behave as a function of N and the time t , for both initial conditions. For this purpose, we define the error Σ as

$$\Sigma(N, t) = \sqrt{\frac{1}{n} \sum_{\alpha=1}^n [r(y_{\alpha}, t) - r_{\text{num}}(y_{\alpha}, t)]^2}, \quad (91)$$

where n is the number of points on a grid $\{y_{\alpha}\}$ at which we numerically computed the rank field (typically $500 \leq n \leq 2000$), $r(y_{\alpha}, t)$ is the predicted rank field at those points, and $r_{\text{num}}(y_{\alpha}, t)$ is the numerical rank field at y_{α} . In Fig. 8 we have plotted $\Sigma(N, t)$, on a ln-ln scale, as a function of N for different initial profiles at different times. For the square initial condition with $l = 10$, we see that $\Sigma(N, t)$ decays with N as a power law N^{-a} , where we measure $\frac{1}{2} < a < 1$.

V. CONCLUSION

In this paper we have studied the out-of-equilibrium Langevin dynamics of N particles in one dimension, which interact only via the linear one-dimensional repulsive Coulomb potential and which are thus allowed to cross. We have focused on an initial condition where all the particles are at the origin at time $t = 0$. As time increases the gas expands. We have shown that there are three distinct regimes in time, separated by two characteristic times. In regime I, i.e., $t < t_1^* = T/(cN)^2$, the particles perform essentially independent Brownian diffusion. At $t = t_1^*$, the particles start experiencing

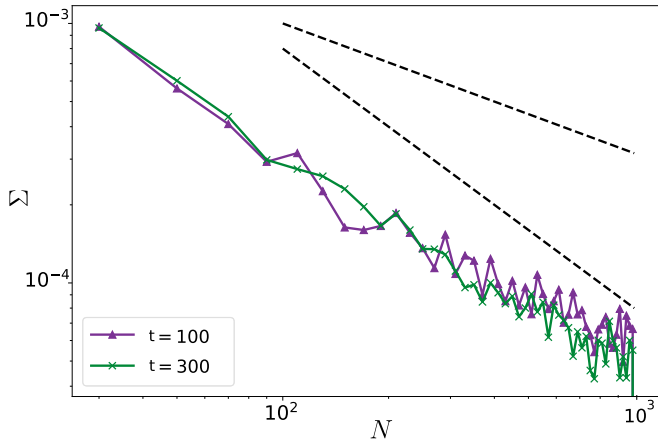


FIG. 8. Fluctuations of the rank field as measured by $\Sigma(N, t)$ defined in (91). We plotted the numerical data for Σ as a function of N in ln-ln scale for $n = 500$ and two different times $t = 100$ and 300 . We have checked that the number of points n on the grid [see Eq. (91)] does not affect significantly the data. Here we fixed $\gamma = 1$ and $T = 1$ and we averaged over 10^4 realizations of the noise. At time zero we start from the square initial condition with $l = 10$. The dashed lines are guides to the eyes and have slopes of $-\frac{1}{2}$ and -1 , respectively.

the long-range interaction and for $t > t_1^*$ the size of the gas increases linearly approximately to $2cNt$; this is the beginning of regime II. A plateau forms in the particle density, with boundary layers of size $\sqrt{2Tt}$ whose shape we have explicitly computed using a relation with the Burgers equation. In this regime II the gas is still dense and the particles still experience many mutual crossings. Finally, as $t \geq t_2^* = T/c^2$ one enters regime III, where the system is a dilute expanding crystal where the particles are well separated. We have studied regime III at long time due to an exact formula obtained from the Bethe ansatz which we analyzed using a saddle-point method. The time-dependent particle distribution shows a remarkable analogy with the one that describes the equilibrium jellium model in the presence of a quadratic well with a time-dependent curvature. This allowed us to quantify the fluctuations of the displacements in the expanding crystal, which are Gaussian and of $O(\sqrt{t})$ to leading order. Interestingly, there are additional $O(1)$ subleading non-Gaussian fluctuations which we obtained exactly. These additional correlations are purely dynamical in origin and do not have any counterpart in the equilibrium jellium model.

There are many interesting questions which remain to be studied. One is the role of the initial conditions. Presumably, in regime III, the analogy with the equilibrium jellium model and the leading Gaussian fluctuations are robust features. However, it is likely that the subleading $O(1)$ non-Gaussian fluctuations for $t \gg T/c^2$ depend on some details of the initial condition. Indeed, we have shown that it is the case for $N = 2$ (see Appendix A 4, where the few lowest cumulants are obtained explicitly for any even initial condition). This shows that the system keeps some memory of the initial condition even at infinite time. It remains to be investigated how this feature extends to any N and whether it persists at large N . Another interesting open matter is the description of the

crossover from regime II to regime III, i.e., times of order $t_2^* = T/c^2$ or smaller. Indeed, as we have shown, the crossover from regime I to regime II for times of order $T/(cN)^2$ can be described using a hydrodynamic approach based on the Burgers equation. This approach however fails as time increases around $t = t_2^*$ when one can no longer neglect the discreteness of the particles. In particular, we expect that the boundary layer at the edges of the plateau in the density becomes quite different from the one computed here. Describing the system in that regime remains an open challenge.

The stochastic dynamics of long-range interacting systems with a nonequilibrium stationary state, such as the Hamiltonian mean-field model, has been studied in the past [26,27]. In contrast, our work concerns the dynamics in a long-range interacting system where there is no stationary state. In the present study we have obtained results in the broader context of interacting Brownian particles with long-range interactions by a combination of analytical methods. A general model much studied recently, in mathematics and physics, mostly at equilibrium [9,28,29], or its quantum generalization [30] is the so-called Riesz gas in one dimension where the repulsive interaction potential behaves as a power law of the distance of approximately $|x_i - x_j|^{-s}$. The case $s = -1$ corresponds to the Coulomb interaction studied here and the case $s = 0$ is the logarithmic gas. The out-of-equilibrium dynamics for general s has not been addressed much (apart of course from $s = 0$ and Dyson's Brownian motion [31]) with the exception of a very recent work [32], where the case $s > 0$ was studied using hydrodynamics methods. The present work opens the way for further investigations of nonequilibrium dynamics for Brownian particle systems with long-range interactions.

ACKNOWLEDGMENTS

P.L.D. and G.S. thank LPTMS for hospitality. We thank the Erwin Schrödinger Institute of the University of Vienna for hospitality during the workshop Large deviations, extremes and anomalous transport in non-equilibrium systems.

APPENDIX A: MORE DETAILS FOR TWO PARTICLES $N = 2$

1. Solution from the Laplace transform

For two particles one can solve directly the problem using the Laplace transform (as in the Supplemental Material of [18] but for $c > 0$). Noting that $x(t) = \frac{1}{2}[x_1(t) + x_2(t)]$ and $y(t) = x_2(t) - x_1(t)$, the center of mass performs an independent unit Brownian motion $\dot{x}(t) = \xi(t)$, while the relative coordinate evolves as

$$\dot{y} = 2c \operatorname{sgn}(y) + 2\eta(t), \quad (\text{A1})$$

where $\eta(t)$ is an independent unit of white noise. Its probability density $P(y, t)$ then evolves according to

$$\partial_t P = 2\partial_y^2 P - 2c\partial_y[\operatorname{sgn}(y)P], \quad (\text{A2})$$

starting with the initial condition $P(y, 0) = \delta(y)$. Introducing the Laplace transform $\tilde{P}(y, s) = \int_0^{+\infty} dt e^{-st} P(y, t)$, one obtains

$$s\tilde{P} - P(y, 0) = 2\partial_y^2 \tilde{P} - 2c\partial_y[\operatorname{sgn}(y)\tilde{P}], \quad (\text{A3})$$

where $P(y, 0)$ is the initial condition. It is then easy to solve separately for $y > 0$ and $y < 0$. There are two integration constants on both sides. One on each side is set to zero by requiring that $\tilde{P}(y, s) \rightarrow 0$ at $y \rightarrow \pm\infty$ for $s > 0$. Continuity of P at $y = 0$ gives another condition and finally, from integrating (A2) on a small interval around $y = 0$, one obtains the matching condition

$$P'(0^+, t) - P'(0^-, t) - 2cP(0, t) = -\frac{1}{2} \quad (\text{A4})$$

and the same relation holds for the Laplace transforms. This leads to the unique solution

$$\tilde{P}(y, s) = \frac{e^{(c/2)|y|}}{2(c + \sqrt{c^2 + 2s})} e^{-\sqrt{c^2 + 2s}|y|/2}. \quad (\text{A5})$$

Hence

$$P(y, t) = e^{-(c^2/2)t} e^{(c/2)|y|} \mathcal{L}_{s \rightarrow t}^{-1} \frac{1}{2(c + \sqrt{2s})} e^{-\sqrt{2s}|y|/2}. \quad (\text{A6})$$

Note that the prefactor $e^{-(c^2/2)t} e^{(c/2)|y|}$ is exactly the one which appears in the Lieb-Liniger method setting $N = 2$. Inverting explicitly the Laplace transform \mathcal{L} , one finds the formula (14) given in the text.

2. Comparison with the general N formula

Let us rewrite the general formula (12) for $N = 2$, defining $y = x_2 - x_1$ and $x = \frac{x_1 + x_2}{2}$, i.e., $x_2 = x + y/2$ and $x_1 = x - y/2$ as above (with $dx_1 dx_2 = dx dy$). It reads, for $x_1 \leq x_2$, that is, for $y \geq 0$,

$$P(x_1, x_2, t) = e^{(c/2)|y|} e^{-(c^2/2)t} \int_{\mathbb{R}} \frac{dk_1}{2\pi} \int_{\mathbb{R}} \frac{dk_2}{2\pi} \frac{ik_1 - ik_2}{ik_1 - ik_2 + c} \times e^{-t(k_1^2 + k_2^2) + ix(k_1 + k_2) + (i/2)y(k_2 - k_1)}. \quad (\text{A7})$$

Let us define $k_1 + k_2 = k$ and $q = (k_2 - k_1)/2$. The above expression factorizes and one obtains

$$P(x_1, x_2, t) = e^{(c/2)|y|} e^{-(c^2/2)t} \left(\int_{\mathbb{R}} \frac{dk}{2\pi} e^{-t(k^2/2) + ikx} \right) \times \left(\int_{\mathbb{R}} \frac{dq}{2\pi} \frac{-i2q}{-i2q + c} e^{-2tq^2 + iyq} \right). \quad (\text{A8})$$

Hence the center-of-mass motion decouples and one has

$$P(x_1, x_2, t) dx_1 dx_2 = \frac{1}{\sqrt{2\pi t}} e^{-x^2/2t} P(y, t) dx dy, \quad (\text{A9})$$

with, for $y \geq 0$,

$$P(y, t) = e^{(c/2)|y|} e^{-(c^2/2)t} \int_{\mathbb{R}} \frac{dq}{2\pi} \frac{-i2q}{-i2q + c} e^{-2tq^2 + iyq}. \quad (\text{A10})$$

The Laplace transform of this expression with respect to time t reads

$$\tilde{P}(y, s) = e^{(c/2)|y|} \int_{\mathbb{R}} \frac{dq}{2\pi} \frac{-i2q}{-i2q + c} \frac{1}{s + 2q^2 + \frac{c^2}{2}} e^{iyq}. \quad (\text{A11})$$

One has $s + 2q^2 + \frac{c^2}{2} = 2(q - q_+)(q - q_-)$, with $q_{\pm} = \pm \frac{i}{2} \sqrt{2s + c^2}$. Since here $y > 0$ we must close the contour in the upper half plane. The pole at $q = -ic/2$ thus does not

contribute and the pole at $q = q_+$ contributes. We obtain from its residue

$$\begin{aligned} \tilde{P}(y, s) &= ie^{(c/2)|y|} \frac{1}{2(c + \sqrt{2s + c^2})} \frac{-2iq_+}{(q_+ - q_-)} e^{-(y/2)\sqrt{2s + c^2}} \\ &= e^{(c/2)|y|} \frac{1}{2(c + \sqrt{2s + c^2})} e^{-(y/2)\sqrt{2s + c^2}}, \end{aligned} \quad (\text{A12})$$

which, using that the final result must be even in $|y|$, recovers the previous result [see (13) and (A5)].

3. Cumulants of $|y| - 2ct$

To obtain the cumulants of $|y| - 2ct$, one can compute the Laplace transform of the generating function

$$\int_0^{+\infty} dt \int dy P(y, t) e^{\lambda(|y| - 2ct) - st} = \int dy \tilde{P}(y, s + 2c\lambda) e^{\lambda|y|}. \quad (\text{A13})$$

Using the expression (13), expanding in λ , and performing the Laplace inversion, we find the moments, and taking the logarithm we obtain the cumulants. From now on we set $c = 1$ for simplicity and will restore it in the text. One obtains

$$\begin{aligned} \langle |y| \rangle - 2t &= (t + 1) \operatorname{erf}\left(\frac{\sqrt{t}}{\sqrt{2}}\right) - t + \sqrt{\frac{2}{\pi}} e^{-t/2} \sqrt{t} \\ &= 1 + O(t^{-3/2} e^{-t/2}), \end{aligned} \quad (\text{A14})$$

$$\begin{aligned} \langle (|y| - 2t)^2 \rangle &= 2(t^2 + 1) \operatorname{erfc}\left(\frac{\sqrt{t}}{\sqrt{2}}\right) - 2\sqrt{\frac{2}{\pi}} e^{-t/2} \sqrt{t}(t - 1) \\ &\quad + 4t - 2 = 4t - 2 + O(t^{-1/2} e^{-t/2}), \end{aligned} \quad (\text{A15})$$

$$\langle (|y| - 2t)^3 \rangle = 12t + 6 + O(t^{1/2} e^{-t/2}), \quad (\text{A16})$$

$$\langle (|y| - 2t)^4 \rangle = 48t^2 - 48t - 24 + O(t^{3/2} e^{-t/2}), \quad (\text{A17})$$

$$\langle (|y| - 2t)^5 \rangle = 240t^2 + 240t + 120 + o(1), \quad (\text{A18})$$

$$\langle (|y| - 2t)^6 \rangle = 960t^3 - 1440t^2 - 1440t - 720 + o(1). \quad (\text{A19})$$

The first four cumulants are given in the text, and we further obtain by this method the next two cumulants

$$\begin{aligned} \langle (|y| - 2ct)^5 \rangle_c &\simeq 744 + o(1), \\ \langle (|y| - 2ct)^6 \rangle_c &\simeq -7560 + o(1). \end{aligned} \quad (\text{A20})$$

Here and above the terms $o(1)$ are exponentially small corrections in t . We see that although the moments are polynomial in t , the cumulants are simply $O(1)$. Furthermore, there are no power-law corrections of the type $1/t^p$, $p \geq 1$, to either moments or cumulants. Finally, one can check that the cumulants obtained exactly here up to order 6 agree with the general prediction obtained in Sec. III D for $k \geq 3$ (restoring c),

$$\langle (|y| - 2ct)^k \rangle_c = \frac{1}{c^k} (-1)^{k-1} (k-1)! (2^k - 1) + o(1). \quad (\text{A21})$$

4. More general initial conditions

In the Supplemental Material of [18] the solution for $P(y, t)$ for $N = 2$ was obtained for a more general class of initial conditions. The calculation was performed for $c < 0$ (i.e., setting $c = -1$); here we adapt it for $c > 0$, following the same steps.

One considers an initial condition $P(y, 0)$ which is smooth around $y = 0$ (for convenience) and an even function of y . Then $P(y, t)$ is also smooth around $y = 0$ and an even function of y . One again defines the Laplace transform with respect to time, $\tilde{P}(y, s) = \int_0^{+\infty} dt e^{-st} P(y, t)$, and one also defines the half-sided Laplace transform with respect to space, $\hat{P}(\mu, s) = \int_0^{+\infty} dy e^{-\mu y} \tilde{P}(y, s)$ (thus using $\lambda = -\mu$ as compared to the notation used in the preceding section). One also defines $P_0(\mu) = \int_0^{+\infty} dy e^{-\mu y} P(y, 0)$, the half-sided Laplace transform of the initial condition. The normalization condition on the half space implies that $P_0(0) = \frac{1}{2}$ and $\hat{P}(0, s) = \frac{1}{2s}$. Taking the double Laplace transform of Eq. (A3) with respect to x and t then leads to

$$s\hat{P}(\mu, s) - P_0(\mu) = 2\mu(\mu - c)\hat{P}(\mu, s) - 2\tilde{P}'(0, s) - 2(\mu - c)P(0, s). \quad (\text{A22})$$

Integrating (A22) around $y = 0$ leads to the jump condition $P'(0^+, s) - cP(0^+, s) = 0$ and its solution reads

$$\hat{P}(\mu, s) = \frac{P_0(\mu) - 2\mu\tilde{P}'(0, s)}{s - 2\mu(\mu - c)}. \quad (\text{A23})$$

We will use the same condition as was used for $c = -1$ in [18] to determine the unknown function $\tilde{P}'(0, s)$, namely, that the residue of the pole at $s = 2\mu(\mu - c)$ should vanish. Indeed, for $\mu > c$, $2\mu(\mu - c) > 0$ and a pole at $s > 0$ would lead to a growing exponential in time, which is excluded. Hence one has

$$\tilde{P}'(0, s = 2\mu(\mu - c)) = \frac{P_0(\mu)}{2\mu}. \quad (\text{A24})$$

Equivalently, setting $\mu = \mu_s = \frac{1}{2}(c + \sqrt{c^2 + 2s})$ (the positive root), one must have

$$\tilde{P}'(0, s) = \frac{P_0(\mu_s = \frac{1}{2}(c + \sqrt{c^2 + 2s}))}{c + \sqrt{c^2 + 2s}}. \quad (\text{A25})$$

The solution is thus

$$\hat{P}(\mu, s) = \frac{1}{s - 2\mu(\mu - c)} \times \left(P_0(\mu) - 2\mu \frac{P_0(\frac{1}{2}(c + \sqrt{c^2 + 2s}))}{1 + \sqrt{c^2 + 2s}} \right). \quad (\text{A26})$$

Let us now compute the cumulants of $|y| - 2ct$. We again use the Laplace transform in time of the cumulant generating function

$$\begin{aligned} & \int_0^{+\infty} dt \int_{-\infty}^{+\infty} dy P(y, t) e^{-\mu(|y| - 2ct) - st} \\ &= \int_{-\infty}^{+\infty} dy \tilde{P}(y, s - 2c\mu) e^{-\mu|y|} \\ &= 2\hat{P}(\mu, s - 2c\mu). \end{aligned} \quad (\text{A27})$$

Let us set from now on $c = 1$ (which means lengths are in units of $1/c$ and time in units of $1/c^2$). Let us define the moments $m_k(t) = \langle (|y| - 2ct)^k \rangle$ and denote by $\tilde{m}_k(s)$ their Laplace transform in time and by $\kappa_k(t)$ the cumulants. We then have

$$\tilde{m}_k(s) = 2(-1)^k \partial_{\mu}^k \big|_{\mu=0} \hat{P}(\mu, s - 2\mu). \quad (\text{A28})$$

To extract the long-time behavior, we perform the small- s expansion for each moment. For instance, we find

$$\tilde{m}_1(s) = \frac{2}{s} [\hat{P}_0(1) - \hat{P}'_0(0)] + \hat{P}'_0(1) - \hat{P}_0(1) + O(s), \quad (\text{A29})$$

which implies that

$$\begin{aligned} m_1(t) &= 2[\hat{P}_0(1) - \hat{P}'_0(0)] + f_1(t), \\ \int_0^{+\infty} dt f_1(t) &= \hat{P}'_0(1) - \hat{P}_0(1), \end{aligned} \quad (\text{A30})$$

where $f_1(t)$ decays to zero at infinity. Hence the $O(1)$ constant in the first cumulant reads

$$\kappa_1(t = +\infty) = 2[\hat{P}_0(1) - \hat{P}'_0(0)] = \langle y + e^{-y} \rangle_0, \quad (\text{A31})$$

where $\langle \dots \rangle_0$ means the average with respect to the initial condition $P(y, 0)$. We recover $\kappa_1(t = +\infty) = 1$ in the limit where $P(y, 0) = \delta(y)$. We see that $\kappa_1(t = +\infty)$ depends on the initial condition. Next we obtain

$$\tilde{m}_2(s) = \frac{4}{s^2} + \frac{2}{s} [2\hat{P}'_0(1) + \hat{P}''_0(0) - 2\hat{P}_0(1)] + O(s^0), \quad (\text{A32})$$

which leads to

$$m_2(t) = 4t + \langle y^2 - 2(1 + y)e^{-y} \rangle_0 + o(t). \quad (\text{A33})$$

Thus we find that the $O(1)$ constant in the second cumulant $\kappa_2(t) = 4t + \tilde{\kappa}_2(t)$ reads

$$\tilde{\kappa}_2(t = +\infty) = \langle y^2 - 2(1 + y)e^{-y} \rangle_0 - \langle y + e^{-y} \rangle_0^2 \quad (\text{A34})$$

and we recover $\tilde{\kappa}_2(t = +\infty) = -3$ in the limit where $P(y, 0) = \delta(y)$. The third and fourth moments are

$$\begin{aligned} m_3(t) &= 12t \langle y + e^{-y} \rangle_0 + \langle y^3 + 3e^{-y}(y^2 + 2y + 2) \rangle_0 \\ &+ o(t), \end{aligned} \quad (\text{A35})$$

$$\begin{aligned} m_4(t) &= 48t^2 + 24t \langle y^2 - 2e^{-y}(y + 1) \rangle \\ &+ \langle y^4 - 4e^{-y}(y^3 + 3y^2 + 6y + 6) \rangle + o(t), \end{aligned} \quad (\text{A36})$$

from which we obtain the third and fourth cumulants, which have heavy expressions not displayed here. We check that all positive orders in t cancel in the k th cumulant, $k \geq 3$, which thus goes to a $O(1)$ constant $\kappa_k(t = +\infty)$ at long time. These $O(1)$ constants carry information, up to infinite time, about some details of the initial condition.

APPENDIX B: MORE ON THE CUMULANTS FROM THE SADDLE POINT

The saddle-point method used in Sec. III D would predict a power law in time corrections to the cumulants, but already for $N = 2$ we know that these do not exist. Let us focus on $N = 2$. To understand this apparent paradox, let us go one step

back and start again from the formula (A10) (setting $c = 1$ for simplicity here),

$$\langle e^{\lambda y} \rangle = 2 \int_0^{+\infty} dy e^{(\lambda+1/2)y} e^{-t/2} \int_{\mathbb{R}} \frac{dq}{2\pi} \frac{-i2q}{-i2q+1} e^{-2tq^2+iyq}. \quad (\text{B1})$$

Instead of performing the saddle point on q and then performing the saddle point on the resulting expression (as we did in Sec. III D), let us simply rewrite (A10) using the shifted variables $y = 2t(1+2\lambda) + \hat{y}$ and $q = \frac{i}{2}(1+2\lambda) + \hat{q}$. We obtain

$$\langle e^{\lambda y} \rangle = 2 \int_{-2t(1+2\lambda)}^{+\infty} d\hat{y} \int_{\mathbb{R}} \frac{d\hat{q}}{2\pi} \frac{1+2\lambda-2i\hat{q}}{2+2\lambda-2i\hat{q}} e^{2\lambda t+2\lambda^2 t-2t\hat{q}^2+i\hat{y}\hat{q}}. \quad (\text{B2})$$

Note that the integration contour of \hat{q} was $\mathbb{R} - \frac{i}{2}(1+2\lambda)$ but we brought it back to \mathbb{R} since the pole at $q = -i/2$ is not crossed along the way (provided $1+2\lambda > 0$). Note that this formula is *exact*; no saddle point has been made. Now we split the integral over \hat{y} in two pieces, i.e., we write $\int_{-2t(1+2\lambda)}^{+\infty} d\hat{y} = \int_{-\infty}^{+\infty} d\hat{y} - \int_{-\infty}^{-2t(1+2\lambda)} d\hat{y}$. In the first piece we use $\int_{-\infty}^{+\infty} d\hat{y} e^{i\hat{y}\hat{q}} = 2\pi \delta(q)$ and we obtain [formally the second piece corresponds to $y < 0$ in (B1)]

$$\langle e^{\lambda y} \rangle = e^{2\lambda t+2\lambda^2 t} \left(\frac{1+2\lambda}{1+\lambda} - 2 \int_{-\infty}^{-2t(1+2\lambda)} d\hat{y} \times \int_{\mathbb{R}} \frac{d\hat{q}}{2\pi} \frac{1+2\lambda-2i\hat{q}}{2+2\lambda-2i\hat{q}} e^{-2t\hat{q}^2+i\hat{y}\hat{q}} \right). \quad (\text{B3})$$

The idea is that the second piece is exponentially small at long time. For instance, for $-2t(2+2\lambda) < \hat{y} < -2t(1+2\lambda)$ one can evaluate the integral over \hat{q} by a saddle-point method, with a saddle point at $\hat{q} = i\frac{\hat{y}}{4t}$. This leads to

$$\int_{\mathbb{R}} \frac{d\hat{q}}{2\pi} \frac{1+2\lambda-2i\hat{q}}{2+2\lambda-2i\hat{q}} e^{-2t\hat{q}^2+i\hat{y}\hat{q}} \simeq \frac{1}{\sqrt{8\pi t}} e^{-\hat{y}^2/8t} \frac{1+2\lambda+\frac{\hat{y}}{2t}}{2+2\lambda+\frac{\hat{y}}{2t}}. \quad (\text{B4})$$

A similar estimate can be obtained for $\hat{y} < -2t(2+2\lambda)$. Hence the final integral over \hat{y} is dominated by its upper bound and is thus of order $e^{-(t/2)(1+2\lambda)^2}$ with algebraic prefactors. This gives an exponentially small correction to the cumulants, of order $e^{-c^2 t/2}$ (restoring c), which is indeed what is obtained by an exact calculation. Note that the exponentially small correction term in (B3) comes from trajectories which cross each other, which become subdominant for $c^2 t \gg 1$. Finally,

these calculations can be generalized to any N , although we will not display it here.

APPENDIX C: ASYMPTOTIC BEHAVIOR OF THE SOLUTION OF THE BURGER'S EQUATION

To study the boundary layer of the density $\rho(x, t)$ in (87) near its right edge, let us recall some useful formulas for the δ initial condition, namely,

$$r(x, t) = -\frac{T}{\gamma} \partial_x \ln[f(x, t) + f(-x, t)],$$

$$f(x, t) = e^{-\gamma x/2T} \operatorname{erfc}\left(\frac{\gamma t - x}{2\sqrt{Tt}}\right), \quad (\text{C1})$$

which we have slightly simplified. Let us focus near the right edge at $x = \gamma t$ and set $x = \gamma t + y\sqrt{Tt}$. Then we find

$$f(x, t) = e^{-\gamma^2 t/2T - \gamma y\sqrt{t}/2\sqrt{T}} \operatorname{erfc}\left(-\frac{y}{2}\right), \quad (\text{C2})$$

$$f(-x, t) = e^{-\gamma^2 t/2T - \gamma y\sqrt{t}/2\sqrt{T}} e^{-y^2/4} \frac{\sqrt{T}}{\gamma\sqrt{\pi t}} \times \left[1 - \frac{y\sqrt{T}}{2\gamma\sqrt{t}} + O\left(\frac{1}{t}\right) \right]. \quad (\text{C3})$$

Hence, for $t \gg T/\gamma^2 = T/(cN)^2$ and $y = O(1)$ we see that the first term dominates. Hence, in that limit we have

$$r(x, t) = \frac{1}{2} - \frac{\sqrt{T}}{\gamma\sqrt{t}} \partial_y \ln \left[\operatorname{erfc}\left(-\frac{y}{2}\right) \right] = \frac{1}{2} - \frac{\sqrt{T}}{\gamma\sqrt{t}} \hat{r}(y),$$

$$\hat{r}(y) = \frac{e^{-y^2/4}}{\sqrt{\pi} \operatorname{erfc}\left(-\frac{y}{2}\right)}, \quad (\text{C4})$$

which describes the boundary layer at the right edge. It behaves as $\hat{r}(y) \simeq \frac{y}{2} + \frac{1}{y}$ for $y \rightarrow -\infty$ and hence matches the linear behavior of the plateau. The density at the edge thus takes the boundary layer form

$$\rho(x, t) = \frac{1}{\gamma t} \hat{\rho}\left(\frac{x - \gamma t}{\sqrt{Tt}}\right),$$

$$\hat{\rho}(y) = \frac{e^{-y^2/2} [2 + \sqrt{\pi} e^{y^2/4} y \operatorname{erfc}\left(-\frac{y}{2}\right)]}{2\pi \operatorname{erfc}\left(-\frac{y}{2}\right)^2}, \quad (\text{C5})$$

where the scaling function has the asymptotic behaviors

$$\hat{\rho}(y) = \frac{1}{2} - \frac{1}{y^2} + O\left(\frac{1}{y^4}\right), \quad y \rightarrow -\infty \quad (\text{C6})$$

$$\hat{\rho}(y) = \frac{y}{2\sqrt{\pi}} e^{-y^2/4}, \quad y \rightarrow +\infty. \quad (\text{C7})$$

The boundary layer form of the density thus matches the density of the plateau $\rho(x, t) \simeq \frac{1}{2\gamma t} = \frac{1}{2cNt}$.

- [1] G. B. Rybicki, Exact statistical mechanics of a one-dimensional self-gravitating system, *Astrophys. Space Sci.* **14**, 56 (1971).
 [2] P. H. Chavanis and C. Sire, Anomalous diffusion and collapse of self-gravitating Langevin particles in D dimensions, *Phys. Rev. E* **69**, 016116 (2004).

- [3] P. Kumar, B. N. Miller, and D. Pirjol, Thermodynamics of a one-dimensional self-gravitating gas with periodic boundary conditions, *Phys. Rev. E* **95**, 022116 (2017).
 [4] A. Lenard, Exact statistical mechanics of a one-dimensional system with Coulomb forces, *J. Math. Phys.* **2**, 682 (1961).

- [5] S. Prager, The one-dimensional plasma, *Adv. Chem. Phys.* **4**, 201 (1962).
- [6] R. J. Baxter, Statistical mechanics of a one-dimensional Coulomb system with a uniform charge background, *Proc. Cambridge Philos. Soc.* **59**, 779 (1963).
- [7] D. S. Dean, R. R. Horgan, A. Naji, and R. Podgornik, Effects of dielectric disorder on van der Waals interactions in slab geometries, *Phys. Rev. E* **81**, 051117 (2010).
- [8] G. Tellez and E. Trizac, Screening like charges in one-dimensional Coulomb systems: Exact results, *Phys. Rev. E* **92**, 042134 (2015).
- [9] For a recent review see M. Lewin, Coulomb and Riesz gases: The known and the unknown, *J. Math. Phys.* **63**, 061101 (2022).
- [10] A. Dhar, A. Kundu, S. N. Majumdar, S. Sabhapandit, and G. Schehr, Exact Extremal Statistics in the Classical 1D Coulomb Gas, *Phys. Rev. Lett.* **119**, 060601 (2017).
- [11] A. Dhar, A. Kundu, S. N. Majumdar, S. Sabhapandit, and G. Schehr, Extreme statistics and index distribution in the classical 1d Coulomb gas, *J. Phys. A: Math. Theor.* **51**, 295001 (2018).
- [12] A. Flack, S. N. Majumdar, and G. Schehr, Truncated linear statistics in the one dimensional one-component plasma, *J. Phys. A: Math. Theor.* **54**, 435002 (2021).
- [13] A. Flack, S. N. Majumdar, and G. Schehr, Gap probability and full counting statistics in the one-dimensional one-component plasma, *J. Stat. Mech.* (2022) 053211.
- [14] D. Chafaï, D. García-Zelada, and P. Jung, At the edge of a one-dimensional jellium, *Bernoulli* **28**, 1784 (2022).
- [15] A. D. Banner, R. Fernholz, and I. Karatzas, Atlas models of equity markets, *Ann. Appl. Probab.* **15**, 2296 (2005).
- [16] S. Pal and J. Pitman, One-dimensional Brownian particle systems with rank-dependent drifts, *Ann. Appl. Probab.* **18**, 2179 (2008).
- [17] For RD see Sec. 5.5, and for more general models where the stationary measure has a product form see, e.g., Corollary 4.8 in N. O’Connell and J. Ortmann, Product-form invariant measures for Brownian motion with drift satisfying a skew-symmetry type condition, *ALEA Lat. Am. J. Probab. Math. Stat.* **11**, 307 (2014).
- [18] P. Le Doussal, Ranked diffusion, delta Bose gas, and Burgers equation, *Phys. Rev. E* **105**, L012103 (2022).
- [19] E. H. Lieb and W. Liniger, *Phys. Rev.* **130**, 1605 (1963); E. H. Lieb, *ibid.* **130**, 1616 (1963).
- [20] M. Gaudin, *The Bethe Wavefunction* (Cambridge University Press, Cambridge, 2014).
- [21] A. Borodin and I. Corwin, Macdonald processes, *Probab. Theory Relat. Fields* **158**, 225 (2014).
- [22] C. A. Tracy and H. Widom, The dynamics of the one-dimensional delta-function Bose gas, *J. Phys. A: Math. Theor.* **41**, 485204 (2008).
- [23] K. Kawasaki and T. Koga, Relaxation and growth of concentration fluctuations in binary fluids and polymer blends, *Physica A* **201**, 115 (1993).
- [24] D. S. Dean, Langevin equation for the density of a system of interacting Langevin processes, *J. Phys. A: Math. Gen.* **29**, L613 (1996).
- [25] K. Kawasaki, Microscopic analyses of the dynamical density functional equation of dense fluids, *J. Stat. Phys.* **93**, 527 (1998).
- [26] S. Gupta, T. Dauxois, and S. Ruffo, A stochastic model of long-range interacting particles, *J. Stat. Mech.* (2013) P11003.
- [27] S. Gupta and S. Ruffo, The world of long-range interactions: A bird’s eye view, *Int. J. Mod. Phys. A* **32**, 1741018 (2017).
- [28] S. Agarwal, A. Dhar, M. Kulkarni, A. Kundu, S. N. Majumdar, D. Mukamel, and G. Schehr, Harmonically Confined Particles with Long-Range Repulsive Interactions, *Phys. Rev. Lett.* **123**, 100603 (2019).
- [29] C. W. J. Beenakker, Pair correlation function of the one-dimensional Riesz gas, *Phys. Rev. Res.* **5**, 013152 (2023).
- [30] B. K. S., D. A. Huse, and M. Kulkarni, Spatiotemporal spread of perturbations in power-law models at low temperatures: Exact results for classical out-of-time-order correlators, *Phys. Rev. E* **104**, 044117 (2021).
- [31] M. L. Mehta, *Random Matrices* (Elsevier, Amsterdam, 2004).
- [32] R. Dandekar, P. L. Krapivsky, and K. Mallick, Dynamical fluctuations in the Riesz gas, *Phys. Rev. E* **107**, 044129 (2023).